UC San Diego

UC San Diego Electronic Theses and Dissertations

Title

Atlas-Based Strategies for Identifying Novel Markers of Left Ventricular Remodeling in Repaired Tetralogy of Fallot

Permalink

https://escholarship.org/uc/item/56n938gm

Author

Forsch, Nickolas Ivan

Publication Date

2020

Peer reviewed|Thesis/dissertation

UNIVERSITY OF CALIFORNIA SAN DIEGO

Atlas-Based Strategies for Identifying Novel Markers of Left Ventricular Remodeling in
Repaired Tetralogy of Fallot

A dissertation submitted in partial satisfaction of the
requirements for the degree Doctor of Philosophy

in

Bioengineering with a Specialization in Multi-Scale Biology

by

Nickolas Ivan Forsch

Committee in charge:

       Professor Andrew D. McCulloch, Chair
       Professor Pedro Cabrales
       Professor Sanjeet Hegde
       Professor Jeffrey H. Omens
       Professor James C. Perry
       Professor Robert S. Ross

2020

The Dissertation of Nickolas Ivan Forsch is approved, and is acceptable in quality
and form for publication on microfilm and electronically:

_____

_____

_____

_____

_____
Chair

University of California San Diego

2020

DEDICATION

This dissertation is dedicated to my parents for their constant love, support, and understanding.

EPIGRAPH

A little nonsense now and then
is relished by the wisest men.

Roald Dahl

LIST OF FIGURES

LIST OF TABLES

ACKNOWLEDGEMENTS

this so that they can live a better life and enjoy all that this world has to offer.

The introduction, in part, is a reprint of material submitted for publication: N. Forsch, S. Govil, J.C. Perry, S. Hegde, A.A. Young, J.H. Omens, A.D. McCulloch. Computational analysis of cardiac structure and function in congenital heart disease: Translating discoveries to clinical strategies. *Journal of Computational Science*. The dissertation author is the first author of this review article.

Chapter 1, in full, is a reprint of material as it may appear in: S. Salehyar, N. Forsch, K. Gilbert, A.A. Young, J.C. Perry, S. Hegde, J.H. Omens, A.D. McCulloch. A novel atlas-based strategy for understanding cardiac dysfunction in patients with congenital heart disease. *Molecular and Cellular Biomechanics* 2019; 16(3). The dissertation author is the co-first author of this article.

Chapter 2, in full, has been submitted for publication: N. Forsch, K. Gilbert, A. Suinesiaputra, S. Hegde, J.C. Perry, H. Naryan, A.A. Young, J.H. Omens, and A.D. McCulloch. Statistical shape features associated with progression of left ventricular systolic dysfunction in repaired tetralogy of Fallot. *Journal of Cardiovascular Magnetic Resonance*. The dissertation author is the first author of this article.

Chapter 3, in full, is material in preparation to be submitted for publication: N. Forsch, S. Salehyar, K. Gilbert, A. Suinesiaputra, S. Hegde, J.C. Perry, A.A. Young, J.H. Omens, and A.D. McCulloch. Morphological markers and determinants of left ventricular systolic dysfunction in repaired tetralogy of Fallot. The dissertation author is the first author of this article.

VITA

2013	Bachelor of Science, Washington University in St. Louis
2015–2016	Teaching Assistant, Department of Bioengineering University of California San Diego
2017	Master of Science, University of California San Diego
2014–2020	Graduate Student Researcher, University of California San Diego
2020	Doctor of Philosophy, University of California San Diego

PUBLICATIONS

N. Forsch, K. Gilbert, A. Suinesiaputra, S. Hegde, J.C. Perry, A.A. Young, J.H. Omens, A.D. McCulloch. Statistical shape features associated with progression of left ventricular systolic dysfunction in repaired tetralogy of Fallot. *Journal of Cardiovascular Magnetic Resonance* 2020 (*In review*).

N. Forsch, S. Govil, J.C. Perry, S. Hegde, A.A. Young, J.H. Omens, A.D. McCulloch. Computational analysis of cardiac structure and function in congenital heart disease: Translating discoveries to clinical strategies. *Journal of Computational Science* 2020 (*In review*).

S. Salehyar*, **N. Forsch***, K. Gilbert, A.A. Young, J.C. Perry, S. Hegde, J.H. Omens, A.D. McCulloch. A Novel Atlas-Based Strategy for Understanding Cardiac Dysfunction in Patients with Congenital Heart Disease. *Molecular and Cellular Biomechanics* 2019; 16(3). *indicates shared first authorship*

K. Gilbert, **N. Forsch**, S. Hegde, C. Mauger, J. Omens, J.C. Perry, B. Pontre, A. Suinesiaputra, A.A. Young, A.D. McCulloch. Atlas Based Computational Analysis of Heart Shape and Function in Congenital Heart Disease. *Journal of Cardiovascular Translational Research* 2018; 1-10.

Z. Chen, Q. Guo, E. Dai, **N. Forsch**, & L.A. Taber. How the embryonic chick brain twists. *Journal of The Royal Society Interface* 2016; 13(124): 20160395.

FIELDS OF STUDY

Major Field: Bioengineering with a Specialization in Multi-Scale Biology

ABSTRACT OF THE DISSERTATION

Atlas-Based Strategies for Identifying Novel Markers of Left Ventricular Remodeling in
Repaired Tetralogy of Fallot

by

Nickolas Ivan Forsch

Doctor of Philosophy in Bioengineering with a Specialization in Multi-Scale Biology

University of California San Diego, 2020

Professor Andrew D. McCulloch, Chair

Tetralogy of Fallot (TOF) is the most common form of cyanotic congenital heart disease
(CHD), occurring in approximately 1 out of every 3,500 births. Innovative surgical strategies
have significantly improved early survival, but patients with repaired TOF are at risk of late
complications due to residual structural and electromechanical cardiac malformations. Chronic
right ventricular (RV) volume overload due to pulmonary valve incompetency is a common
problem in repaired TOF, and pulmonary valve replacement can alleviate regurgitation and
normalize RV volume and function. However, left ventricular (LV) systolic dysfunction can
develop in the long-term and has been identified as a risk factor for early morbidity and mortality.

Traditional assessment of LV remodeling and dysfunction for prognostic purposes is limited due to the complex inter-patient variability of LV morphology and the compounding effects of RV dilatation and dysfunction.

In this thesis, we seek to help address the challenges with clinical management of repaired TOF by elucidating patterns of LV remodeling that associate with systolic dysfunction and can provide an indication of further LV deterioration. To this purpose, we use statistical shape analysis to quantify inter- and intra-population variation of LV morphology and systolic function. The aims of this dissertation are to:

1. Characterize the statistical variation of end-diastolic (ED) shape and systolic function in a large cohort of patients with repaired TOF using routinely acquired cardiac magnetic resonance image data;

2. Identify novel features of ED morphology that associate with systolic dysfunction using computational models of LV mechanics informed by patterns discovered in patient data;

3. Test the hypothesis that novel atlas-based features of remodeling are predictive of functional deterioration of the LV.

Here we demonstrated the first derivation and use of an atlas of LV shape of a large cohort of repaired TOF from multi-center cardiac magnetic resonance image data. Abnormal shape features from an asymptomatic reference population associated with global systolic function in our TOF cohort, but were inadequate for assessment of LV functional deterioration; conversely, we found novel LV shape features from the repaired TOF atlas, rather than standard CMR measures or shape features from the reference atlas, to be associated with the change in global systolic function in a longitudinal study. Mechanistic models of systolic mechanics informed by statistical atlases were capable of systematically testing for shape determinants of LV dysfunction, and were used to generate hypotheses of disease mechanisms that would otherwise need to be measured invasively. A more comprehensive assessment of LV morphology in repaired TOF

using statistical shape atlas techniques has the potential to discover hidden patterns of adverse remodeling that contain mechanistic insight and prove valuable for clinical decision-making.

Introduction to the Dissertation

0.1 Abstract

Increased availability and access to medical image data has enabled more quantitative approaches to clinical diagnosis, prognosis, and treatment planning for congenital heart disease. Here we present an overview of long-term clinical management of tetralogy of Fallot (TOF) and its intersection with novel computational and data science approaches to discovering biomarkers of functional and prognostic importance. Efforts in translational medicine that seek to address the clinical challenges associated with cardiovascular diseases using personalized and precision-based approaches are then discussed. The considerations and challenges of translational cardiovascular medicine are reviewed, and examples of digital platforms with collaborative, cloud-based, and scalable design are provided.

0.2 Introduction

The wide-scale availability of large, heterogeneous patient datasets brings new opportunities and challenges to addressing complex problems in clinical medicine. In the field of cardiology, advances in cardiovascular imaging have the potential to enable more quantitative approaches to diagnosis, surgical planning and medical therapies, but much of the information in clinical cardiac imaging data goes under-utilized by routine clinical image assessment methods. In diagnostics, cardiac magnetic resonance (CMR) imaging is not routine in acquired heart diseases but is common in congenital heart disease (CHD), where patients are often very young and repeated exposure to ionizing radiation is contraindicated. Improved availability of clinical datasets for research is accelerating the intersection of medicine and computational science, fostering collaborations within and between the biomedical science, computational science, and clinical communities. Anecdotal and empirical clinical practice is evolving towards evidence-based precision medicine. New innovations and discoveries arising from interdisciplinary collaborations on research that aims to translate from bench to bedside involve technical, regulatory, and ethical hurdles. In this chapter, we discuss the breadth of clinical challenges, research strategies, processes, and impact of translational computational science in the context of clinical management in CHD.

0.3 Tetralogy of Fallot

Tetralogy of Fallot (TOF) is the most common form of cyanotic CHD and is characterized by a specific combination of four anatomic malformations. Originally described by Louis Arthur Etienne Fallot in 1888, the defining features consist of a ventricular septal defect (VSD), a biventricular connection of the aortic root (overriding aorta), obstruction of the right ventricular (RV) outflow tract, and RV hypertrophy [1, 2]. Cardiac malformations present in TOF can have a varying degree of type and severity, which directly impacts the manifestation of the disease and its clinical management. Treatment of TOF in the modern era has evolved from palliative surgery,

involving a systemic artery-to-pulmonary artery shunt during infancy, to complete intracardiac repair, the purpose of which is to improve blood flow to the lungs and preserve separation of oxygenated and deoxygenated blood. Specifically, complete intracardiac repair involves the widening of the narrowed pulmonary blood vessels and closure of the VSD using an atriotomy or ventriculotomy approach. The widening of the RV outflow tract is commonly achieved by performing a transannular patch repair to enlarge the pulmonary annulus, however, patients are prone to a weakening of the pulmonary valve. As an alternative, valve-sparing techniques can be performed to preserve the tissue of the pulmonary annulus by surgical resection of the pulmonary valve tissue in a procedure called a commissurotomy. In some patients, a conduit between the RV and the pulmonary arteries is needed to support pulmonary blood flow. Complete intracardiac repair is typically performed in the first year of life; in cases where the neonate is too weak or small to perform a complete repair, a palliative systemic artery-to-pulmonary artery shunt is placed to increase blood flow to the lungs.

Patients with TOF can develop complications after repair due to residual structural and electromechanical cardiac malformations, including pulmonary valve incompetency, residual VSDs, and RV conduction delay as a result of the altered electrophysiological properties of a VSD patch and surrounding scar tissue. Complications that can arise include arrhythmias, RV aneurysms, and pulmonary regurgitation with subsequent RV volume overload. Long-term monitoring of repaired TOF primarily focuses on RV remodeling as a consequence of RV volume overload. RV dilatation can develop in the presence of pulmonary regurgitation and chronic volume overload, which has been associated with exercise intolerance, atrial and ventricular arrhythmia, and sudden cardiac death [3]. While patients can tolerate RV volume load without symptoms for many years, the risk of heart failure increases in the third and fourth decades of life [4]. The RV under chronic volume load initially undergoes a compensatory response characterized by an increase in end-diastolic (ED) volume and myocardial hypertrophy, followed by a failure of compensatory mechanisms, resulting in continued dilatation and a lack of further hypertrophy. If left untreated, myocardial remodeling can progress into RV failure due

3

to impaired contractility and irreversible myocardial injury. Patients with chronic pulmonary regurgitation can undergo pulmonary valve replacement (PVR) to alleviate RV volume overload and halt and reverse RV dilatation.

RV dysfunction is a consequence of adverse RV remodeling and can also contribute to left ventricular (LV) dysfunction due to adverse ventricular-ventricular interactions [5]. Direct mechanical interactions occur due to a shared interventricular septum (IVS), myofibers, pericardium, and coronary blood flow. Studies have demonstrated a leftward shift in the IVS due to interactions at the IVS [6, 7]. Furthermore, a causal relationship has been demonstrated in studies where alleviation of RV volume loading via PVR has resulted in improved LV function [8]. While clinical management of repaired TOF is fundamentally focused on the RV, long-term biventricular consequences of the disease demand a comprehensive monitoring of biventricular remodeling and function.

0.4   Computational Analysis of Congenital Heart Disease

Clinical management of CHD, characterized by the presence of cardiac malformations at birth, has transformed greatly over the past few decades. Clinical innovations for complex CHD over several decades have resulted in a shift to more definitive treatment strategies that have increased early survival rates and extended life expectancy into adulthood. Complete surgical repair of complex cardiac malformations in diseases such as TOF has resulted in twenty-five-year survival of upwards of 95% [9]. In spite of the abundance of successful outcomes after complete repair, patients with TOF are commonly burdened with chronic pulmonary valve insufficiency and RV volume overload owing to residual structural and electromechanical malformations [10]. Interventions such as pulmonary valve replacement (PVR) can help alleviate pulmonary insufficiency, but surgical procedures carry risk, and long-term outcomes after PVR remain inconsistent [11, 12, 13, 14]. To closely monitor the long-term sequelae in TOF, clinical management depends on the routine use of non-invasive medical imaging, including echocardiography and CMR [15].

Imaging enables the quantitative assessment of regional and global cardiac structure and function, and with its greater accessibility and use in practice, measurable indices with prognostic value have been derived and used to assess adverse remodeling of the heart and guide therapy [16, 17].

In spite of the wealth of information available from a single CMR image dataset, its value towards clinical decision-making has limitations. Assessment of medical image data requires specialized technical personnel, accurate and reliable software to analyze images, and time to perform the analysis and interpret the results. Additionally, current standards for the quantitative assessment of cardiac structure and function have been under-utilized for prognostic purposes. It is clear that clinical practice surrounding the treatment and management of CHD could benefit from the translation of computational tools that: 1) accelerate the process of extracting relevant information from image data; 2) condense complex cardiac features into interpretable and quantifiable measures; and 3) provide new insight into disease mechanisms and clinical outcome predictors.

Various computational techniques exist to extract three-dimensional (3D) measurements of cardiac anatomy and morphology from medical images commonly by image segmentation. These techniques can be entirely manual, requiring a human analyst to trace features of interest from a set of images, semi-automated, such as guide-point modeling, or entirely automated, such as via deep learning-based algorithms. Fully manual techniques are time-consuming but can be highly accurate depending on the training of the analyst, whereas fully automated techniques are faster but are prone to error depending on the training of the algorithm. Compared with fully automated techniques, manual or semi-automated segmentation methods often require significant local expert knowledge to achieve an acceptable accuracy; in clinical practice, this translates to extra costs and time. In contrast, once a reliable automated algorithm has been trained and validated, its use can support local expertise and can be scaled up for widespread deployment.

CMR imaging is highly suitable for quantitative cardiac analysis and many advances in semi-automated and fully automated segmentation have been based on data from this imaging modality due to its widespread use [18]. Previously, semi-automated techniques such as guide-

point modeling relied on the interactive placement of "guide-points" to anatomical landmarks or features of an image to constrain the alignment of a 3D model to a patient-specific anatomy [19]. More recent efforts have focused on cardiac image segmentation using deep learning, enabled by more advanced computer hardware and the increased availability of training data. Deep learning-based models typically use artificial neural networks (e.g., CNNs, FCNs, U-nets, and RNNs) to develop a general-purpose learning procedure in end-to-end fashion [20]. However, the accuracy and reliability of deep learning models is contingent on access to a large image dataset that is representative of the clinical cohort of interest. Rigorous validation methods are essential for the translation of machine learning for cardiac image analysis into clinical practice, and significant coordinated effort has been made. For example, Bhuva et al. [21] compared the precision of machine learning and humans across multiple diseases, institutions, scanner manufacturers, and scanner types. Additionally, while automated and semi-automated segmentation methods have already reached clinical CMR analysis software programs, validation is still in-progress for anatomically challenging regions of the heart, such as the RV and atria, but recent studies have made strong advances [22, 23, 24]. These segmentation methods are even more limited in the analysis of complex CHD anatomies, such as dextro-transposition of the great arteries where the RV is the system ventricle. Development of large databases of both anatomically normal and abnormal hearts will help solve these challenges by providing training and validation data for deep learning models. Segmentation and analysis methods have been successfully developed using large pre-clinical epidemiological studies including the Multi-Ethnic Study of Atherosclerosis and the UK Biobank [25, 26]. In order to translate these methods to specific clinical cohorts, some adaptation and retraining is required to cope with the altered geometry and function seen in CHD patients.

Large enough collections of cardiac image segmentations can be used to generate statistical atlases of morphological and functional variations within a population using unsupervised machine learning methods such as principal component analysis (PCA). PCA, when used on anatomically co-registered models of cardiac shape, can reduce thousands of input variables

6

into a much smaller set by decomposing the variability of the data into a set of orthogonal components ranked by the amount of variance explained. As a result, a collection of models from a patient population is characterized by a reduced set of orthogonal components and their associated variance. In turn, each patient's cardiac shape can be represented by a condensed set of statistical measures (e.g., Z-scores) that each quantify the distance from the population mean and individually represent the variation of hundreds of input variables. This process has advantages from a clinical, technical, and physiological perspective: the simplification of complex, multi-dimensional data from CMR images into interpretable features allows for more quantitative assessment of potentially important markers of patient status and outcomes while providing qualitative representations of biological phenomena that may contain mechanistic insight. Furthermore, patient-specific measures derived from statistical atlases of cardiac structure and function allow for inter- and intra-cohort comparisons that can assess how abnormal an individual is relative to a healthy population and any differences from patients with the same disease and similar interventions. Technically, databases can be composed of much smaller files with numeric data type rather than hundreds to thousands of gigabytes of image data.

Patient-specific metrics quantified from statistical cardiac atlases can also be used to discriminate other relevant clinical factors, such as global ventricular function, specific disease phenotypes, and differences in treatment strategies using unsupervised learning algorithms, including K-means clustering and partial least squares regression (see Figure 0.1 for an overview). These analyses can provide the foundation by which new hypotheses are generated and can be used to discover valuable predictors of clinical outcomes that can be validated using supervised learning methods, such as regularized kernel learning algorithms [27, 28]. All of the aforementioned machine learning tools can be easily implemented using Python bindings to well-known machine learning libraries, e.g. Tensorflow (https://www.tensorflow.org) and PyTorch (https://pytorch.org). In practice, cardiac atlases of ventricular geometry have been used in healthy, CHD, and cardiovascular disease populations to associate shape and structure with cardiovascular risk factors [29, 30, 25, 31, 26]. In studies of TOF, statistical atlases have been

used to investigate the 3D shape of the RV and predict ventricular remodeling [32, 33].

The statistical atlas-based approach is just one of many being undertaken in the field of computational cardiac modeling. Multi-scale models of biomechanics and electrophysiology can build on the information gained from statistical atlases to further test for relationships between observable features of cardiac structure and function from imaging and intrinsic myocardial material properties and electrical activation patterns, which can otherwise only be measured invasively [34]. This analysis enables the exploration of the mechanisms that give rise to differences in patient outcomes that are either resultant or independent from easily measurable markers. The "Your Personal Virtual Heart" project takes another approach that aims to employ patient-specific computational models rather than population-based models to improve ventricular tachycardia risk stratification in TOF patients via simulated electrophysiological pacing studies [35, 36]. Others are modeling the great vessels and adjacent vasculature rather than the heart itself using computational fluid dynamics with fluid-structure interactions to quantify how hemodynamics are altered as a result of surgical interventions, such as a Fontan procedure or placement of a shunt, in a variety of CHD patient cohorts [37]. These models are made with the open-source software package SimVascular, which provides a complete pipeline from image segmentation to patient-specific blood flow simulation and analysis [38]. Strategies such as the "digital twin" that synergize mechanistic and statistical approaches have the potential to accelerate the translation of discovery to precision medicine in the clinic [39].

0.5 Translation Process

An overview of the translation process in cardiovascular medicine is shown in Figure 0.2. Data acquisition and hosting are at the core of computational research and have several additional requirements in the context of translational medicine. These requirements primarily involve the security and privacy of any collected human subject data, e.g. medical images, medical reports, lab reports, and omics data. The Health Insurance Portability and Account-

ability Act (HIPAA) maintains that all patient data must be anonymized such that original patient data is unlinked to data presented in research. Accomplishing this requires significant resources particularly when accounting for the numerous data types involved, each of which have their own data format and associated metadata that may also vary between medical institutions [40, 41]. Additionally, re-identification of patient data may be necessary to relate any discoveries back to the patient, which poses its own challenges [42]. There are several publicly available tools to remove identifying information from patient datasets (e.g., electronic medical records) such as Google's Cloud Healthcare API (https://cloud.google.com) and the Anonymization toward De-identification (deid) Python module (https://pypi.org); however, the lack of a single tool endorsed at the community level makes it difficult to maintain a consistent standard for anonymization between research groups and clinical institutions around the world. In addition to data acquisition, several cloud-based platforms with HIPAA-compliant, data-sharing capabilities and collaborative code generation are being developed to accelerate the discovery and dissemination of landmark findings from computational studies. Platforms such as iDASH (integrating data for analysis, anonymization, and sharing), previously supported by the NIH National Center for Biomedical Computing, aim to provide computational biomedical researchers access to data, software, and a high-performance computing environment for studies that focus on various health conditions spanning multiscale biology [43]. Another such platform funded by the American Heart Association Precision Medicine Platform is the Cardiac Atlas Project (https://www.cardiacatlas.org), which is a large-scale database of cardiac images and associated clinical data that facilitates collaborative statistical analysis of regional heart shape and wall motion for normal and pathological patient populations [44]. The Cardiac Atlas Project database also promotes public standards for data anonymization by providing tools for de-identification of DICOM, the standard file format of medical images. Merging data repositories and tools for CMR image analysis, cloud-based platform Arterys allows for rapid analysis of image data using advanced computational algorithms. Using the cloud-based platform and computing resources, clinicians are able to quantitatively analyze four-dimensional blood flow in approximately ten

minutes (https://arterys.com). In order to establish these digital platforms, privacy-protecting analytics and secure data-sharing methods must be implemented such that all data contributed and accessed have a minimal risk of disclosure of sensitive information. One of the biggest limitations in scaling up these endeavors, however, is that all collaborating institutions have to ensure that any contributed or accessed data is approved by each local IRB and other institutional guidelines, and conforms to the standards set by the platform.

Successful implementation of new initiatives for knowledge discovery and data-driven decision-making inevitably improves the clinical understanding of disease outcomes and associated risk factors while also illuminating the mechanisms of disease progression. Altogether, these platforms contribute to precision medicine, an approach that relies on scientifically-derived biomarkers via machine learning techniques applied to large-scale datasets, rather than classical diagnostic markers. The integration of these platforms and associated workflows in the clinic, however, is a more complicated endeavor. Typically, big-data population studies in translational computational science are conducted with retrospective data, often resulting in heterogeneous datasets. While any novel discoveries or insights from these studies may be scientifically validated, they need to be clinically validated through prospective clinical studies to ensure that patient outcomes are significantly improved. Consenting and enrolling patients at scale to assess the effectiveness of novel biomarkers requires significant resources both in time, as the follow-up time period for these patients could be several years, and funding, to cover the costs of intermittent exams during this period [45, 46]. After demonstrating success in small clinical studies, these software-based workflows may be subject to FDA approval via the Software as a Medical Device (SaMD) pathway prior to widespread use (https://www.fda.gov). Only after passing all of these regulatory hurdles can the discoveries and insights from these platforms be integrated with clinical workflows and hospital-side technologies, such as the electronic medical record and PACS (photo archiving and communication system) information systems. This integration will also require significant community effort in order to ensure that distributed systems are able to interact with each other efficiently while maintaining HIPAA-compliance. The effort will also

10

require the development of extensive documentation and training seminars to educate clinicians on how to use platform tools, interpret results, and communicate results back to patients in a comprehensible way.

0.6 Impacts and Lessons Learned

The impact of this work on the fields of biomedical engineering and computational sciences is traditionally measured by the number of high-impact publications, adoption of methods by other research groups and institutions, and the securing of funding by national agencies to continue improving the technology towards shareable industry standards [47]. In the context of translational medicine, however, there are additional ways to measure impact that are clinically motivated, including impact on patient management and outcomes, changes to the gold standard of care, and widespread adoption of these tools and techniques across hospital networks [48]. In the case of platform technologies such as Arterys and the Cardiac Atlas Project, impact can also be measured by overall size of the data repositories, the number and variety of data contributors and users, and the robustness of software-based tools and documentation.

One of the main challenges when it comes to performing translational research is that its two primary components – the development of technology in the lab and the implementation of that technology in the locale – are often considered in isolation rather than as a single, complete strategy. Typically, scientific funding sources for the development of technology is provided to answer important questions with novel approaches, while funding for its implementation and continual support is typically left out. This is partially influenced by the difference in timelines and incentives of these two components of translational computational science. The timeline for technology development is often much shorter and has a more immediate observed impact by way of publications and conferencing within the scientific community. The timeline for the implementation of the technology, however, can take much longer and requires significantly more resources for expansion and continual support, such as web-based hosting fees in the case

11

of platform technologies. Furthermore, the measurable impact on health and healthcare is far more drawn out considering the regulatory hurdles that have to be crossed prior to adoption at the bedside. One way to encourage the implementation of a technology alongside its development with the potential to generate sustainable revenue is by funding agencies prioritizing research projects that have a high potential to generate and protect intellectual property, such as via patenting, and ensure that the funding agency retains exclusive licensing rights to the technology. In this manner, the successful implementation of the technology in a healthcare system can be financially sustainable and has potential to generate revenue for supporting similar endeavors. The key to the success of this approach is an emphasis on observed impact both scientifically and medically.

The emergence of translational computational science in the field of cardiology can transform clinical decision-making. Computational modeling of individual or population-wide cardiac structure and function has allowed us to capture more relevant and quantifiable information from routinely-collected health data that is normally unrecognized. While technological and scientific validation is ubiquitous in the laboratory, significant resources and effort are required to interface new technology within the medical community, gain acceptance, and integrate with clinical practice. Research planning with a clear strategy and pathway to translation can help focus efforts across scientific and medical communities towards the common goal of redirecting and improving medical practice.

0.7   Aims of the Dissertation

The goal of this dissertation was to gain new insight into the markers, mechanisms, and predictors of LV systolic dysfunction in repaired TOF. A deeper understanding of remodeling patterns and mechanisms in TOF will translate to improved clinical prognosis and, ultimately, prevention of poor late outcomes. For this purpose, we used statistical shape analysis of patient-specific models derived from CMR image data to qualitatively and quantitatively characterize the
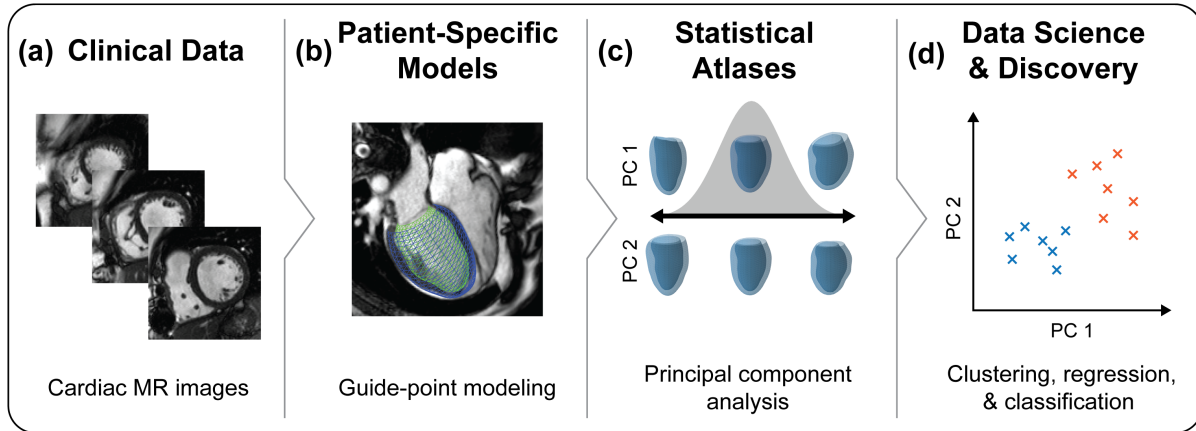
Figure 0.1. Overview of the process of discovering novel predictors of clinical outcome from routinely acquired image data. (a) Cardiac MRI datasets are used to generate (b) patient-specific models of ventricular shape and function via guide-point modeling or automated image segmentation techniques. (c) Principal component analysis can be used to quantify the statistical variation of cardiac shape in a patient population and derive novel markers of remodeling. (d) Machine learning methods can be used to discover associations of atlas-derived markers with patient outcomes and support clinical decision-making. MR, magnetic resonance.

variation in LV ED shape and associate baseline measures with longitudinal changes in systolic function.

0.8 Acknowledgements
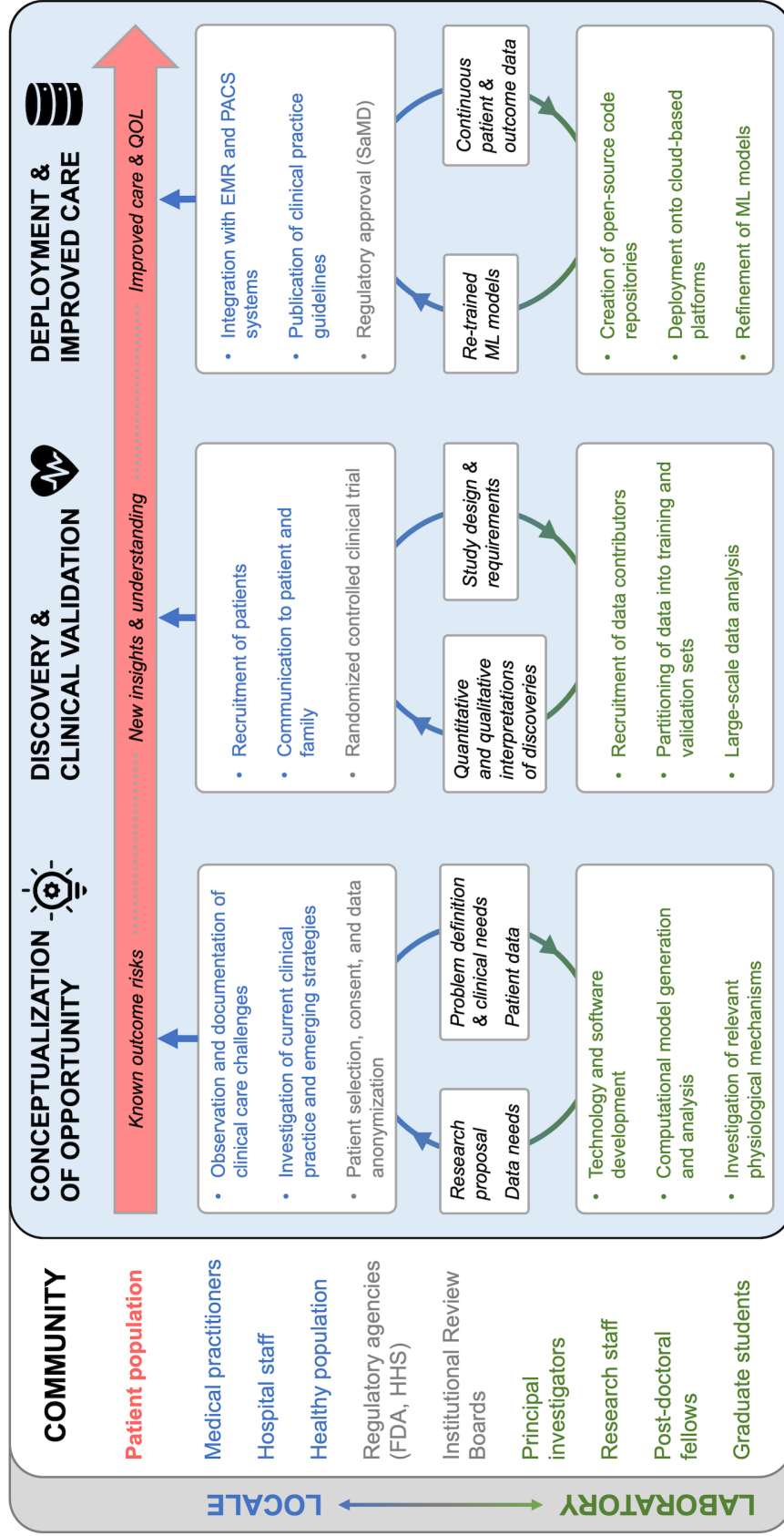
Figure 0.2. Translational process of computational cardiology highlighting the interplay between the laboratory (e.g., research facility and computing resources) and the locale (point of care). EMR, electronic medical record; PACS, picture archiving and communication system; SaMD, Software as a Medical Device; ML, machine learning.

Chapter 1

A Novel Atlas-Based Strategy for Understanding Cardiac Dysfunction in Patients with Congenital Heart Disease

1.1 Abstract

Tetralogy of Fallot (TOF) is the most common form of cyanotic congenital heart disease. Infants diagnosed with TOF require surgical interventions to survive into adulthood. However, as a result of postoperative structural malformations and long-term ventricular remodeling, further interventions are often required later in life. To help identify those at risk of disease progression, serial cardiac magnetic resonance (CMR) imaging is used to monitor these patients. However, most of the detailed information on cardiac shape and biomechanics contained in these large four-dimensional (4D) data sets goes unused in clinical practice for lack of efficient and comprehensive quantitative analysis tools. While current global metrics of cardiac size and function, such as indexed ventricular mass and volumes, can identify patients at risk of further complications, they are not adequate to explain the underlying mechanisms causing the postoperative malfunctions, and help cardiologists plan optimal personalized treatments. We are proposing a novel approach that uses 4D ventricular shape models derived from CMR imaging exams to generate statistical atlases of ventricular shape and finite-element models of ventricular biomechanics to identify specific features of cardiac shape and biomechanical

properties that explain variations in ventricular function. This study has the potential to discover novel biomarkers that precede adverse ventricular remodeling and dysfunction.

1.2 Introduction

Congenital heart disease (CHD) is the most common type of birth defect. With the improvements in the management of CHD, infants born with these cardiac malformations can now survive into adulthood [49]. Among these congenital heart defects, tetralogy of Fallot (TOF), characterized by four anatomical defects (pulmonary stenosis, right ventricular hypertrophy, ventricular septal defect, and an overriding aorta), is the most common heart lesion accounting for approximately 10% of all congenital cardiac malformations [50]. These issues are typically addressed by surgery after birth, however, these surgical repairs often lead to pulmonary regurgitation (PR) by the second or third decade of life that can lead to right ventricular (RV) enlargement and dysfunction, consequent left ventricular (LV) remodeling and, ultimately, heart failure [51, 52, 53, 54].

In patients with repaired tetralogy of Fallot (TOF), cardiac magnetic resonance (CMR) imaging is the gold standard for clinical decision support because of its ability to quantify ventricular size and function [55]. Despite the wealth of information available in four-dimensional (4D) cardiac shape and wall motion in CMR, only a small set of measurements of global cardiac volume and size are used by cardiologists for determining the time of further interventions in repaired TOF patients. Shape atlases derived from surface registration methods provide a high spatial resolution of cardiac morphology. The application of dimensionality-reduction techniques, such as principal component analysis (PCA), to three-dimensional (3D) ventricular shape can derive orthogonal modes of shape and function in an unbiased framework. Recent studies of ventricular morphology and function have adopted statistical shape modeling as a method of atlas generation in both congenital and asymptomatic cohorts, demonstrating an association of atlas-based shapes to risk factors and dysfunction [26, 30, 34].

This chapter is a demonstration of the methods developed to understand the underlying mechanisms causing the postoperative malfunctions in repaired TOF by using the 4D information in CMR. In section 2, the statistical atlas approach and ventricular finite-element (FE) modeling

are briefly described. In section 3, preliminary results related to the clinical application of statistical shape atlases have been included. The results of the ventricular FE modeling and more elaborate and advanced results of the statistical atlases of ventricular shape will be included in our future publications.

1.3 Methods

1.3.1 Study Cohort and Clinical Data

CMR image data of patients with repaired TOF were obtained from the CHD Cardiac Atlas Project (CAP) database (http://www.cardiacatlas.org), which integrates clinical data and derived shape models of patients with congenital defects. This study used retrospective CMR data from 99 patients with repaired TOF. CMR datasets were obtained with informed consent and de-identified and contributed to the CHD CAP database following approval of the local institutional review boards at the University of California San Diego (La Jolla, CA, USA) and University of Auckland (Auckland, New Zealand). CMR measurements of the LV were made using custom software (CIM, Auckland, New Zealand). RV volume and function data from CMR measurements were collected for a subset of 11 patients with TOF who had serial CMR data.

1.3.2 Statistical Atlases of LV Shape

Methods for generating shape models of the LV and statistical atlases of ED shape variation have been previously described in [26] and [30]. The process involves a geometric fit analysis using guide-point modeling software (CIM, Auckland, New Zealand). For each case, a 3D shape model is fit to endocardial and epicardial surface contours, and overall model alignment is achieved using fiducial anatomical landmarks. An atlas of LV ED shape was derived by applying PCA to 3D coordinate points from the endocardial and epicardial surfaces of the shape models from the TOF patient group. This study used a previously derived atlas of LV ED shape in an asymptomatic reference population for comparison to the congenital atlas [26].

1.3.3 Analysis of Shape Atlas and Clinical Data

To quantify differences between ED shape modes derived in the atlas of patients with TOF and those from the asymptomatic reference atlas, we used an analysis from Krzanowski to calculate vector projections between the first twenty principal components of both atlases [56]. This calculation produces a scalar between 0, indicating orthogonal shape modes, and 1, indicating equivalent shape modes.

A subset of 11 TOF patients were used in a longitudinal study of LV and RV remodeling. To explore the potential value of novel atlas-based shape modes in predicting changes in LV and RV volume and function, regression analysis was used to test for correlations between various baseline parameters and the change in indexed RV and LV end-diastolic volume (EDVi), end-systolic volume (ESVi), stroke volume (SVi), and ejection fraction (EF). The baseline parameters consisted of RV and LV CMR parameters as well as shape mode z-scores from the TOF ED atlas. Statistical analyses were performed using R Studio (R Studio Inc., Boston, MA).

1.3.4 Finite-Element Models of Ventricular Biomechanics

Ventricular FE models enable the estimation of muscle passive stiffness, active properties, and wall stresses. In this study, ventricular geometry was generated from epicardial and endocardial surfaces of the atlas-based shapes, and cubic-Hermite FE meshes were generated accordingly. The load-free geometry and passive material properties of the average TOF patient were estimated using the iterative method proposed in [57]. In the strained ED configuration, the active forces will be adjusted such that the ventricular shape and volume from the FE model will match the measured end-systole shape and volume. In this model, the first mode of ED shape from the TOF atlas will be varied to test for potential mechanisms of dysfunction due to variations in this TOF-specific shape mode.

1.4 Results

1.4.1 Comparison Between ED Shape Atlases of the TOF and Reference Groups

An atlas of statistical shape variation at ED was derived using PCA of the LV shapes of the TOF patients, resulting in five shape modes explaining over 75% of total variation in the TOF patients. Systematic comparison of the first twenty ED shape modes of the TOF and control atlases identified the first mode of the TOF group (Figure 1.1) as having the lowest similarity to an ED mode of the control atlas; TOF mode 1 had the highest degree of orthogonality to modes of the reference atlas with a maximum vector projection value of 0.16. This first mode explained 26% of all ED shape variation in the TOF patients.

1.4.2 Prediction of LV and RV Remodeling

The first shape mode of the TOF atlas was the best correlate among all baseline variables for three of the eight response variables (ΔLVESVi, ΔLVEF, and ΔRVESVi) and significantly correlated with four of the eight (ΔLVESVi, ΔLVEF, ΔRVEDVi, and ΔRVESVi; $p < 0.05$) after controlling for age and time between CMR examinations (Table 1.1). The strongest associations were between baseline TOF shape mode 1 and ΔLVESVi ($R^2 = 0.80$, $p < 0.01$) and baseline LVESVi and ΔRVEDVi ($R^2 = 0.80$, $p < 0.01$).

1.5 Conclusions

Shape modeling of the LV in repaired TOF revealed unique modes of ED shape that were often better than conventional CMR parameters in predicting RV and LV remodeling. This study demonstrates the clinical utility of statistical shape modeling in the context of CHD, the ultimate goal of which is to discover novel biomarkers of shape and function that precede long-term adverse ventricular remodeling and dysfunction.

1.6 Acknowledgements

-3 SD   Mean   +3 SD
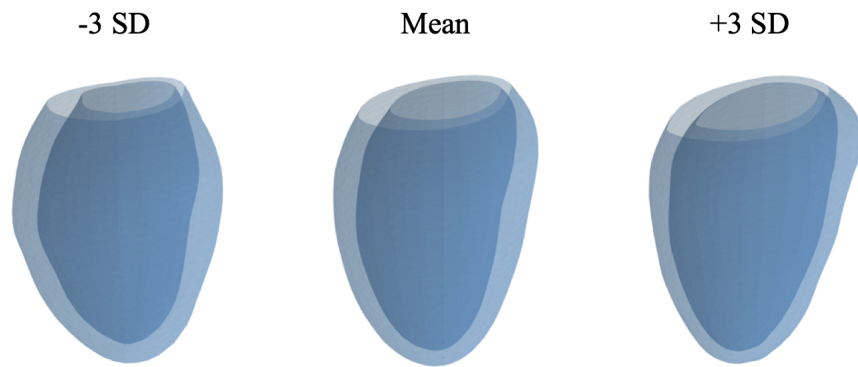
Figure 1.1. Shape variation of the first mode of the TOF end-diastolic atlas. The mean shape and the variation of -3 and +3 standard deviations from the mean are represented. SD is standard deviation.

Table 1.1. Correlation of baseline parameters with changes in ventricular volumes and function

| | | Response Variable‡ R^2 Value | | | | | | | |
Baseline predictor variable	Mean† (n=11)	ΔLVEDVi	ΔLVESVi	ΔLVSVi	ΔLVEF	ΔRVEDVi	ΔRVESVi	ΔRVSVi	ΔRVEF
LVEDVi, mL/m²	83.3 ± 7.7	0.29	0.48	0.11	0.42	0.75*	0.51	0.75*	0.41
LVESVi, mL/m²	30.8 ± 5.3	0.28	0.49	0.29	0.59	**0.80****	0.55	**0.78***	0.44
LVSVi, mL/m²	52.5 ± 5.4	0.34	0.39	0.14	0.28	0.54	0.37	0.56	0.45
LVEF, %	63.1 ± 4.6	0.30	0.45	**0.34**	0.56	0.67*	0.47	0.65*	0.47
RVEDVi, mL/m²	140 ± 32	0.28	0.39	0.09	0.28	0.53	0.41	0.59	0.53
RVESVi, mL/m²	62.6 ± 17	0.33	0.48	0.08	0.32	0.53	0.44	0.61	**0.59**
RVSVi, mL/m²	77.7 ± 18	0.34	0.40	0.12	0.29	0.52	0.38	0.56	0.46
RVEF, %	55.6 ± 5.1	**0.70***	0.77	0.14	0.42	0.53	0.44	0.60	0.57
TOF ED mode 1	0.40 ± 0.6	0.44	**0.80****	0.09	**0.65***	0.68*	**0.74***	0.56	0.47

*p < 0.05, **p < 0.01
† Values represented as Mean ± SD.
‡ Bold values indicate the best predictor variable for each response variable.

24

Chapter 2

Statistical Shape Features Associated with Progression of Left Ventricular Systolic Dysfunction in Repaired Tetralogy of Fallot

2.1 Abstract

2.1.1 Background

Patients with repaired tetralogy of Fallot (TOF) are at risk of developing left ventricular (LV) systolic dysfunction late after surgical repair, the mechanisms of which are poorly understood. Although the need for management of long-term right-ventricular (RV) disease is common in TOF, patients would also benefit from better assessment of LV remodeling before overt systolic dysfunction becomes manifest. The objective of this study was to identify novel markers of LV remodeling that associate with deterioration of LV systolic function in a cohort of repaired TOF subjects with cardiac magnetic resonance (CMR) evaluation.

2.1.2 Methods

We analyzed cross-sectional CMR imaging data of 99 subjects with repaired TOF (22 $\pm$ 15 years, 63% male) and a sub-cohort of 20 subjects at longitudinal follow-up (median inter-study duration 2.1 years). All subjects were assigned scores for modes of LV end-diastolic

(ED) geometric variation from separate statistical shape atlases generated from two populations: 1) an asymptomatic reference population (61.5 ± 10.2 years, 48% male) with normal cardiac anatomy and 2) the TOF cohort. Subject-specific scores of shape modes were used to discover by regression analysis LV shape abnormalities that predict changes in LV ejection fraction (EF).

2.1.3 Results

Compared to the reference population, TOF subjects showed highly significant abnormalities in indices of sphericity, wall mass, atrioventricular valve plane orientation, and septal wall morphology ($p < 0.0001$). These abnormalities were also associated with differences in TOF subject LVEFs ($p < 0.01$). Two shape modes derived from the TOF-specific shape atlas were markedly better correlates of decreased LVEF ($p = 0.013$) than standard CMR parameters of remodeling or any shape mode derived from the reference atlas. Subjects with a more conical overall LV shape, greater curvature of the septal wall and apex, and lower wall mass near the apex were more likely to experience subsequent longitudinal deterioration of LVEF.

2.1.4 Conclusions

Novel shape markers of LV remodeling from a statistical atlas of CMR-derived models of repaired TOF subjects were better correlates of reduced LV systolic function than standard clinical indices in a repaired TOF cohort. While further studies are required to validate these findings in an independent cohort, atlas-based metrics of LV shape may help to identify patients at risk of deterioration of LV function and shed light on RV-LV interactions in TOF.

2.2 Background

Long-term management of repaired tetralogy of Fallot (TOF) remains a challenge due to residual electromechanical and structural lesions [58]. Monitoring and management of the right ventricle (RV) is typically the primary clinical focus, as persistent pulmonary regurgitation and subsequent RV dilatation are common [15, 59]. Although RV disease is a well-established potential consequence of TOF, left ventricular (LV) systolic dysfunction, manifested by diminished LV ejection fraction (LVEF) and regional function, is also prevalent in this population after years of subclinical development [52, 60, 61]. Furthermore, LV systolic dysfunction is associated with poor outcomes, including death and sustained ventricular tachyarrhythmia [54, 62, 63, 64, 65]. As overt LV systolic dysfunction may be a late finding with potentially irreversible remodeling, there is a need for an earlier and more sensitive means of disease detection and predictors of disease progression.

Adverse structural remodeling of the LV may precede systolic dysfunction, but it is poorly detected by standard indicators of myocardial remodeling, such as indexed volume and mass [66, 67, 68, 69]. A more comprehensive and quantitative assessment of LV shape that takes better advantage of the three-dimensional information in cardiac magnetic resonance (CMR) imaging could improve prediction of disease progression more than conventional CMR-derived metrics. Statistical cardiac shape atlases provide an unbiased and efficient method for quantifying regional variations in cardiac shape and function by condensing complex features from high-dimensional, image-based datasets into interpretable features. Statistical distributions of atlas-based features, used to quantify remodeling and characteristics of asymptomatic and disease populations, have been applied to congenital heart disease (CHD) [26, 70, 25, 34, 30]. The present study uses a shape atlas approach to discover new relationships between LV geometric remodeling and systolic dysfunction in repaired TOF.

The objectives of the study were: (1) quantify specific and novel features of adverse LV remodeling in subjects with repaired TOF using statistical shape atlases; and (2) determine

whether these novel features are predictive of subsequent deterioration of LV systolic function. To achieve these objectives, we created a CMR image dataset from a cross-sectional and longitudinal cohort of subjects with TOF for analysis.

2.3   Methods

2.3.1   Subjects and Data Collection

This study analyzed retrospective CMR datasets from subjects with repaired tetralogy of Fallot acquired for clinical purposes at Rady Children's Hospital San Diego (San Diego, California, USA) and the Auckland Heart Center (Auckland, New Zealand). All images and data were obtained as part of the Cardia Atlas Project (CAP) and used in accordance with local institutional review boards (IRB) at the University of California, San Diego ("The Cardiac Atlas Project", La Jolla, California, USA) and the University of Auckland (Auckland, New Zealand) [44]. Serial CMR data was obtained for a subset of subjects with TOF to analyze longitudinal changes in LV shape and function. Only subjects with two CMR examinations at least six months apart *without* interval pulmonary valve replacement (PVR) between examinations were included in the longitudinal study. Data from a reference population of 1,991 asymptomatic adults with anatomically normal hearts were used for comparison [26].

Standardized procedures from the Cardiac Atlas Project were used for the contribution, de-identification, classification, and sharing of image data. Relevant demographic and clinical data were obtained and de-identified for each subject from medical records associated with CMR datasets. CMR image data obtained from the Auckland Heart Center did not have additional clinical data, and the timing and type of primary repair was unknown in these subjects.

2.3.2   Cardiac MR Image Acquisition and Analysis

Images were acquired using 1.5 T magnetic resonance imaging scanners, including Phillips Intera (Phillips Healthcare, Best, The Netherlands), Siemens Avanto (Siemens Medical

Systems, Erlangen, Germany), and GE Discovery and Signa (GE Healthcare, Milwaukee, USA). Each subject underwent standard functional CMR examination within the scope of clinical practice. Two-dimensional cine images used in this study were acquired using steady state free precession imaging and were prospectively or retrospectively gated with acquisition of at least thirty reconstructed phases per RR interval. Short axis slices spanning from the base to the apex were acquired. At least two long-axis imaging planes (two-chamber, four-chamber, or LV outflow tract) were acquired through valve annuli.

Quantitative measurements of the LV from CMR images were obtained using custom guide-point modeling software (CIM, Auckland, New Zealand). Methods for generating shape models of the LV for asymptomatic and congenital cases have been previously described [26, 30]. Briefly, a geometric fit analysis was performed for each subject by an expert analyst. A 3D shape model was interactively customized by least-squares optimization to a combination of guide points provided by the analyst and computer-generated points from an edge detection algorithm. Overall alignment of the model to each case was achieved using fiducial anatomical landmarks at the mitral valve and the insertion points of the RV free wall at the inter-ventricular septum. In all cases, papillary muscle mass was excluded from the LV mass. For the longitudinal sub-cohort, both RV and LV volumes were re-analyzed using standard contouring methods (Medis Suite 3.1, Leiden, The Netherlands), secondary to LV measurements obtained using custom software for validation purposes. RV volumes derived from standard methods are reported in this study. Additionally, pulmonary insufficiency was assessed by a pulmonary regurgitant (PR) volume fraction derived from phase contrast flow imaging.

2.3.3   Analysis of Left Ventricular Shape Using Statistical Shape Atlases

Principal component analysis (PCA) was used to extract "modes" of LV geometry in each clinical population based on the statistical variation of the input data. The collective set of shape modes derived from PCA define a statistical shape atlas. To prepare the PCA input data, the fitted LV shape models were sampled at the endocardial and epicardial surfaces to generate a

set of unique 3D coordinate points per model. Registration of the model to fiducial landmarks eliminates any variations due to cardiac position and orientation. Variations in LV size due to height are removed using a normalizing scale factor. More details on PCA atlas creation can be found in Farrar *et al.* [30]. Subject-specific scores obtained for each principal component quantitatively represented the distance of each shape from the mean. This study used both a previously derived atlas of LV ED geometry from an asymptomatic adult population as well as an LV atlas of ED geometry from ninety-nine TOF subjects to quantify the statistical variation within our cohort [26, 30]. LV models of ED shape from the TOF subjects were projected onto the atlas of the asymptomatic reference population to generate subject-specific Z-scores for each mode, yielding an indication of geometric abnormalities. Similarly, Z-scores were derived from projecting LV models of TOF subjects onto the TOF LV shape to quantify how much a subject's LV differed from the TOF group mean.

In order to assess whether differences in ED shape between the repaired TOF and reference groups were due to age-related factors, the distributions of mode scores between TOF subjects with ages overlapping with the reference group (ages 45 to 73 years) and an age-matched sample of subjects from the reference group (ages 45 to 73 years) were compared. Random sampling was used to generate an age-matched group from the reference population; briefly, for each subject with TOF, a subject from the reference group with a similar age was randomly sampled. This procedure was repeated thirty times and mode scores were averaged over repetitions to obtain a mean shape for each age-matched reference subject. Z-scores from these groups were also compared to shape distributions for TOF subjects of age less than 45 years to determine differences in shape by age within the TOF group.

2.3.4 Statistical Analysis

Characteristics and measured CMR parameters of the asymptomatic and TOF subjects were summarized using descriptive statistics. Continuous variables were described as means and standard deviations (SD) or as medians and ranges, unless otherwise indicated. Normality

of data was assessed using the Shapiro-Wilk test. An F-test was used to determine equality of variances between the TOF and reference population for modes of ED shape. An unpaired t-test was used to test for equality of group means for atlas mode scores; if group variances were not assumed to be equal, a Welch's unpaired t-test was used.

Statistical correlation among variables in this study was assessed using Pearson's r correlation coefficient between two independent variables or using linear regression analysis for multiple independent variables. One-way ANOVA was used to test for differences in means between LVEF classes for various LV measurements, including standard remodeling indices and shape mode Z-scores. LVEF class for TOF subjects was designated based on quartiles of the TOF subjects: below 25th percentile (below Q1, low LVEF), between 25th and 50th percentiles (Q1 to Q2), between 50th and 75th percentiles (Q2 to Q3), and above the 75th percentile of LVEF (above Q3, high LVEF).

In the longitudinal study of the TOF sub-cohort, one-way ANOVA was used to test for differences in CMR parameters between subjects whose LVEF improved *versus* those whose function deteriorated over the inter-study period. Multiple linear regression was used to test for correlations between various baseline parameters from CMR and the change in indexed LV volumes and mass between the two measured time points. The baseline variables included standard clinical indices of volume and mass and atlas-based modes of ED shape. Age at initial examination and the time between examinations were included in the regression models to control for differences. To test whether modes of ED shape derived from the statistical variation of a larger sample of TOF subjects would be more informative of the long-term changes in global systolic function, we included these modes in the analysis and compared them to the standard clinical indices and shape modes from the control atlas.

Statistical analyses were performed using the SciPy Python library (https://www.scipy.org). Statistical significance was assessed at the 0.05 level, except for tests with multiple comparisons of independent measures in which there was no pre-established hypothesis of significant associations. In these cases, a *post hoc* Holm-Bonferroni correction was used with a

0.01 level of significance in which hypotheses are rejected one at a time based on α divided by the number of remaining hypothesis tests [71]. All statistical tests were two-sided.

2.3.5 Calculation of the Difference in Shape Between the TOF and Reference Populations

For each ED shape mode, the fraction of total shape difference between TOF and reference subjects was calculated by dividing the mean score for a mode by the sum of the mean scores for all modes. This allows for ranking of shape modes based on the proportion of shape difference explained by each mode. The mean difference in overall ED shape for each TOF subject was calculated as the Mahalanobis distance metric, shown in Equation 1 [72]. This metric represents the distance between a point and a distribution; here, the LV shape of an TOF subject and the shape distribution of the reference population. This distance metric, d, is calculated for each patient, with $N = 1{,}990$, as follows:

$$d = \sqrt{\sum_{k=1}^{N} \frac{s_k^2}{\sigma_k}} \tag{2.1}$$

where s_k is the score and σ_k is the variance for principal component k.

2.4   Results

2.4.1   Study Population

This study included a total of 99 subjects with repaired TOF (mean age 22.4 ± 15.4 years; 63% male). A summary of clinical characteristics and CMR measurements for the reference and TOF groups is shown in Table 2.1. Compared to the reference population (mean age 61.5 ± 10.2 years; 48% male), global LV function was lower in the TOF group (mean LVEF 63% versus 52%). For the sub-cohort in the longitudinal study, mean age at time of imaging and at time of primary repair was similar to the entire TOF group mean. Pulmonary insufficiency was high in this sub-cohort on average, as indicated by a high mean PR fraction of 37% (Table 2.1).

2.4.2 TOF Atlas of Left Ventricular End-Diastolic Shape

The geometric variation of the first five modes of the repaired TOF ED atlas are shown in Figure 2.1. These modes explained 69% of the total shape variation in the TOF cohort. Qualitatively, the first mode represents variation in wall thickness and the antero-septal wall morphology; the second mode represents variation in overall LV size and conicity; the third mode primarily represents variation in the diameter of the base; the fourth mode represents variation in septal wall morphology (concave *versus* convex); and the fifth mode represents variation in the wall volume of the interventricular septum and the valve plane orientation.

2.4.3 Analysis of End-Diastolic Shape in TOF Relative to the Reference Atlas

Out of the twelve modes of the reference atlas that explain 30% of the average differences in TOF subjects, shape mode variances were significantly larger than asymptomatic subjects for all but three ($p < 0.01$; Figure 2.2). Furthermore, mean ED shape mode scores were significantly different from the reference population mean for all but the first mode, which generally represents overall LV size ($p < 0.01$). The third ED mode ("ED3"), which is visually associated with sphericity (defined by the ratio of the long axis to the short axis) and valve plane orientation, accounted for 10% of the total difference in TOF ED shape from the reference group mean.

The first five shape modes from the reference atlas that account for the highest proportion of difference from the reference mean are represented in Figure 2.2B. The primary observable differences relative to the control mean were related to overall LV sphericity (ED3), conicity (ED9), wall thickness (ED8), valve plane orientation (ED2 and ED3), and overall curvature of the long axes between the base and apex (ED8 and ED10). On average, the LVs of TOF subjects are more spherical, have a more antero-lateral facing valve plane, have a flatter septal wall, and have reduced wall mass, particularly of the septal wall and apex.

Age-related differences in ED shape were analyzed for modes accounting for the largest difference between the TOF and reference groups (Figure 2.3). Significant differences in shape

mode 1, representing overall LV size, were found between the youngest TOF group and the older TOF and reference groups. However, this mode was not different between the age-matched TOF and reference groups. For modes 3, 9, and 10, significant differences in shape were still present between the TOF and reference sample groups after removing age differences, and no significant differences were found between the youngest and oldest TOF groups ($p < 0.05$). For mode 8, no significant difference was found between the age-matched TOF and reference groups. In contrast, significant differences were found between the youngest and oldest TOF groups and the age-matched TOF and reference groups for mode 2.

2.4.4   Differences Between the TOF and Reference Atlases

Shape modes from the reference atlas were insufficient to explain the variation in LV ED shape in TOF: the first twenty modes of the normal atlas explained 93% of variance in the normal subjects but only explained 50% of variance in the TOF subjects. Additionally, TOF LVs contained 73% more variance in ED shape than the reference group. Differences were observed in the features of shape variation, particularly of septal wall morphology and wall volume, between the top-ranked modes of the TOF atlas and the most abnormal modes of the reference atlas (Figure 2.1; Figure 2.2B).

2.4.5   Association of Shape Atlas Modes with Global Systolic Function in TOF

On average, TOF subjects with LVEF below the median (52.4%) had a greater difference in ED shape from the reference group mean than subjects with LVEF above the median. The difference in LV shape for subjects in the high ($>75^{th}$ percentile) and low ($<25^{th}$ percentile) LVEF groups was greater: the Mahalanobis distance metric was 29.5 *versus* 24.2, respectively, although the differences in LVEF means were not statistically significant ($p = 0.061$). The mean shape mode Z-scores of the high and low LVEF groups were also compared (Figure 2.4). For the majority of shape modes, subjects with a low LVEF had more normal shape mode scores than

those with a high LVEF on average. Of the twenty most abnormal ED modes in TOF subjects, mode 3 and mode 20 had statistically significant differences in mode score means ($p = 0.010$ and 0.0042, respectively; Figure 2.4B-C). Out of the first ten shape modes from the TOF atlas, only mode 6 was associated with LVEF group ($p < 0.01$; Figure 2.4D). A lower LVEF was associated with increased sphericity, higher wall mass, a more lateral-facing valve plane, greater curvature along the septal wall, and bulging of the anterior wall. Differences in standard clinical indices of remodeling were analyzed for the low and high LVEF groups (Figure 2.4A). Of the four indices studied (LV end-diastolic volume index (LVEDVi), LV end-systolic volume index (LVESVi), LV mass index (LVMi), and LV mass-to-volume ratio), the only significant difference found was of LVESVi ($p < 0.0001$).

2.4.6 Longitudinal Changes in TOF Sub-Cohort

A summary of the differences in age and CMR parameters over the follow-up period is provided in Table 2.2. The mean inter-study duration was 2.8 ± 1.6 years. The change in RV and LV ejection fraction was mixed in TOF subjects, with ranges of -15 to 16 and -14.6 to 5.3%, respectively. Changes in LVEF strongly correlated with changes in LVESVi ($r = -0.89$, $p < 0.0001$) but did not significantly correlate with changes in LVEDVi ($r = -0.34$, $p = 0.14$) or PR fraction ($r = 0.31$, $p = 0.19$).

No significant differences in baseline clinical or CMR variables were found between subjects whose LVEF increased and those whose LVEF decreased over the inter-study period (Table 2.3). In contrast, differences in ED shape related to mitral valve annulus diameter and orientation as well as regional wall volume near the base and apex showed differences between these subjects (Figure 2.5). Those whose LVEF decreased qualitatively showed a larger degree of geometric changes over time, despite a similar mean time between CMR examinations between the positive and negative ΔLVEF groups (2.6 and 2.9 years, respectively). Visually, primary changes in LV shape for subjects whose LVEF decreased were a reduced tilt in the valve plane relative to the long axis, reduced septal wall curvature, and increased conicity, in addition to

overall increased wall mass (Figure 2.5). Of the standard CMR parameters measured, the change in LVEDVi ($p = 0.04$), LVESVi ($p < 0.001$), and LVEF ($p < 0.001$) were significantly different between groups (Table 2.3).

2.4.7 Association of Diminishing Left Ventricular Function with Atlas Scores

Changes in LVEF were best explained by an ED shape mode from the TOF atlas at baseline, rather than a conventional global measure of volume or mass or a mode of shape from the reference atlas (Table 2.4). The best correlate of the change in LVEF from the set of standard CMR parameters was baseline LVEF ($p = 0.309$), whereas the best correlates from the set of shape atlas predictor variables was the baseline Z-score for shape mode 7 of the TOF atlas ($p = 0.018$) followed by the baseline Z-score for mode 8 of the TOF atlas ($p = 0.024$). Additionally, combining both TOF atlas modes 7 and 8 in a multiple regression model improved the prediction of the change in LVEF (adjusted $R^2 = 0.43$; $p = 0.013$). The LVs of subjects whose LVEF decreased over the follow-up duration had more conical shape overall, a more pointed apex morphology, a flatter antero-septal wall, and lower wall mass from the mid-ventricle to the apex (Figure 2.6).

In addition to the baseline Z-score, changes in LVEF over time also correlated with changes in the Z-score of TOF atlas mode 7 ($r = -0.57$, $p = 0.008$). The LVs of subjects who experienced a decrease in EF became more spherical rather than conical, developed a flatter apex, increased in wall mass from the mid-ventricle to the apex, and decreased in wall mass from the mid-ventricle to the base.

2.5 Discussion

The causes of left ventricular systolic dysfunction in patients with repaired TOF are poorly understood, despite a 20% prevalence of acquired impaired LVEF and an association with poor outcomes [52, 54, 62]. In this study, statistical atlases of LV ED shape were applied to

subjects with repaired TOF to quantify specific abnormal features of LV remodeling relative to a reference group of clinically asymptomatic adults with normal heart anatomy and within the TOF group itself. Features of ED shape related to sphericity, conicity, septal wall morphology, and orientation of the valve plane were associated with LVEF in subjects with TOF. In our longitudinal study of a sub-cohort of subjects with serial CMR data, we found the best baseline predictor of the future change in LVEF was a mode of shape from a TOF LV atlas, rather than standard clinical indices of remodeling or modes of shape from the asymptomatic reference atlas. These findings suggest that quantification of LV shape and function in repaired TOF using novel atlas-based measures may provide earlier, more sensitive markers of adverse remodeling that precede significant LV systolic dysfunction.

2.5.1 Left Ventricular Structure and Function in Repaired Tetralogy of Fallot

This study demonstrates a novel approach to fully characterizing specific quantifiable abnormalities of LV shape in TOF relative to an asymptomatic population. We found that over 30% of the average geometric differences from the normal control mean were explained by just five ED shape modes. The primary observable differences from normal were increased sphericity, increased conicity, septal wall morphology, and reduced wall mass, particularly of the septal wall and apex (Figure 2.1). LV sphericity is well-characterized feature of adverse remodeling in both asymptomatic and cardiovascular disease (CVD) populations [29, 73, 74]. Similarly, LV conicity has been shown to predict adverse remodeling following acute myocardial infarction, with higher baseline conicity associated with increasing LVEDV and decreasing LVEF [75]. Overall lower wall mass and thickness, combined with higher ED volume compared to the normal group could indicate a failure of compensatory remodeling mechanisms, such as concentric or eccentric hypertrophy, to maintain systolic pump function in many of the TOF subjects. Interestingly, the observed locality of reduced wall volume of the inter-ventricular septum and apex overlaps with studies of myocardial fibrosis, both replacement and interstitial, in repaired TOF. Discrete

replacement fibrosis is typically observed in the RV outflow tract and ventricular septal defect in repaired TOF, but has also been reported in the septal insertion points and the LV apex [76, 77]. Additionally, studies of adults with repaired TOF found elevated LV extracellular volume in 13% and 29% of patients, suggesting the presence of myocyte atrophy and diffuse interstitial fibrosis [78, 79]. While fibrosis can be expected after surgical repair, its presence at the septal insertion points implicates adverse interventricular coupling mechanics as a potential mechanism, which may be reflected by our observed shape variations.

In this study, approximately two thirds of subjects with repaired TOF had at least mild LV systolic dysfunction ($<55\%$), similar to a study by Andrade et al. [69]. The association of specific modes of ED shape from the normal atlas with LVEF highlights the interplay of LV structure and function. Z-scores for specific shape modes showed differences in TOF between high and low LVEF groups. On average, features of ED shape related to sphericity, septal wall morphology, and orientation of the valve plane were significantly different between these subjects. Those with lower LVEF had more abnormal shapes, as indicated by Z-scores further from the mean. Higher sphericity in TOF subjects was associated with lower EF, which has also been observed in a population free of known CVD [29].

We discovered additional morphometric features associated with lower EF that may be specific to this CHD population; an ED shape mode which primarily captures variation in septal wall curvature and overall morphology associated with LVEF class in the subjects with TOF (Figure 2.2). Greater septal wall curvature relative to the LV long axis associated with a lower EF. Qualitatively, this is in contrast to a study by Li *et al.* who found reduced septal curvature, as measured from a short axis view at ED, to be related to adverse LV systolic strain, mechanical dyssynchrony, and twist [80]. Variations in septal wall morphology may be attributable in part to variations in RV volume loading and the degree of interventricular dyssynchrony. Whether global systolic dysfunction is a result of structural ventricular remodeling or the dysfunction perpetuates adverse remodeling remains unknown and warrants further investigation.

A clear linear relationship exists between RVEF and LVEF [3]. Interactions at the

interventricular septum (IVS) affected by shared myofibers, pericardium, and coronary blood flow can cause a leftward shift in the IVS [6, 7]. A causal relationship has been demonstrated in studies where alleviation of RV volume loading via pulmonary valve replacement (PVR) has resulted in improved LV function [8]. While the goal of this study was not to directly investigate this interaction, the underlying mechanisms appear to manifest as variations in the shape and systolic function of the LV that were measured. Mechanical and electromechanical aberrations in TOF have been implicated in impaired LV diastolic and systolic function due to LV-RV interactions.

2.5.2 Deterioration of LV Function in Repaired TOF

Several prior longitudinal studies of ventricular remodeling and systolic dysfunction in patients with repaired TOF have been unsuccessful at identifying baseline predictors of diminishing RV and LV EF. We found baseline Z-scores of modes of ED shape from the TOF LV atlas most strongly predicted the change in LVEF. In a study by Wald *et al.*, baseline clinical parameters and CMR imaging data did not differentiate between patients whose ventricular function was unchanged from those whose function deteriorated over a median time span of 2.2 years [67]. Jing *et al.* examined additional CMR parameters including cardiac strain and mechanical dyssynchrony but did not identify predictors of ventricular deterioration over a mean follow-up duration of 2.9 years [68]. A similar conclusion was found in a more recent study of ventricular strain parameters [81]. Using the same clinical cohort as in Wald *et al.*, in combination with machine learning tools, Samad *et al.* found parameters related to LV function and PR fraction to be the best baseline predictors of subsequent ventricular deterioration [82]. The discovery of parameters of LV function being the most useful for predicting deterioration in both the RV and LV is interesting, as it highlights the value of monitoring the LV in a primarily right-sided disease. In this study and others, an inverse relationship was found between baseline LVEF and deterioration of function, *i.e.*, higher baseline LVEF more commonly resulted in a decrease of global systolic function [68, 82]. Clinical management may benefit from additional,

novel measures of LV remodeling, such as those identified through computational cardiac atlases in this study.

2.5.3   Cardiac Atlases

Development of computational cardiac atlases is enabled by greater accessibility to rich CMR datasets, particularly in the growing TOF and CHD patient population. In this study, we utilized both a normal and a TOF-specific LV atlas to analyze shape in patients with repaired TOF. Reliance solely on a normal atlas to observe primary features of remodeling in a CHD or CVD population can be flawed. This is clearly shown in our TOF cohort, where a shape mode explaining less than 2% of variation in the asymptomatic subjects was highly abnormal and contained nearly six times more variance in TOF. Furthermore, we found that only half of the variance in ED shape in subjects with TOF was explained by the first twenty modes of the reference atlas despite explaining 93% of variance in normal subjects. Nevertheless, comparison of patients with TOF to the reference LV atlas enabled quantification of abnormalities that did associate with LVEF, exemplifying the value of inter-group comparisons as a means to assess function-preserving morphology.

2.5.4   Limitations

Assessment of LV shape is limited by the techniques in our guide-point modeling analysis. The template prolate spheroidal model is based on LV shape and anatomy in a normal population. Development of a more robust template, or one that is specific to TOF morphology, will enable more accurate assessment of 4D (3D+t) shape. Indeed, progress is being made to develop bi-ventricular computational cardiac atlas templates that are specific to CHD populations [34, 83].

The use of a large LV atlas from nearly two-thousand clinically asymptomatic subjects allowed for the characterization of distinct abnormalities in TOF patients. However, subjects from the reference atlas were significantly older on average, and differences in LV shape and systolic mechanics may be convoluted by age differences. While we tested for age-based differences in

shape, the development of a large, normative atlas of LV shape will enable more reliable analyses of individuals who may be at risk of developing LV dysfunction during the early decades of life.

The longitudinal study of a subset of TOF subjects with serial CMR image data used a relatively small sample size, due to limitations of available data. Additionally, there may exist a clinical bias towards patients who are worse off when more frequent CMR examinations are performed. However, we found a fairly even separation of patients whose LV function improved and those whose LV function got worse. The LV volumes and mass for this sub-cohort were measured using two different methods for validation. While we found consistent differences in measured LVEF between the two methods, we concluded that the differences in measured values could be attributed to differences in contouring techniques and measurement error and uncertainty.

2.6   Conclusions

In this cross-sectional cohort of subjects with repaired TOF, abnormalities of LV end-diastolic shape relative to an asymptomatic reference population were associated with global LV systolic dysfunction. In our longitudinal study of twenty TOF subjects, the best baseline correlate with the change in LVEF was an ED shape mode of a repaired TOF LV atlas, rather than standard clinical indices of global remodeling or modes of LV shape from the reference atlas. Shape markers derived from statistical shape atlases may drive hypotheses of disease mechanisms that can be tested with organ-level models of cardiac biomechanics, on an individual or population level. Altogether, the findings of this study highlight the potential importance of monitoring LV morphological remodeling in the presence of repaired TOF as a means to predict and, ultimately, prevent development of systolic dysfunction.

2.7 Acknowledgements

Table 2.1. Clinical characteristics and CMR measurements for subjects in the reference and repaired TOF groups.

	Reference	Repaired TOF	
	All subjects ($n = 1{,}991$)	All subjects ($n = 99$)	Sub-cohort* ($n = 20$)
Characteristics			
Age, y	61.5 ± 10.2	22.4 ± 15.4	19.2 ± 12.3
Age range, y	44 - 84	2 - 73	3.8 - 48.9
Sex, male	957 (48%)	62 (63%)	13 (65%)
Height, m	1.66 ± 0.01	1.54 ± 0.24	1.53 ± 0.23
Weight, kg	76.8 ± 16.5	59.2 ± 29.2	55.0 ± 28.2
BSA, m^2	1.84 ± 0.22	1.56 ± 0.50	1.50 ± 0.49
Age at primary repair, y	-	$0.81 \pm 0.8^{\dagger}$	0.78 ± 0.7
Type of primary repair			
Transannular patch (TAP)	-	23	9
Valve sparing (VS)	-	3	1
Unknown	-	73	10
CMR parameters			
LV end-diastolic volume, mL	125.4 ± 31.2	129.5 ± 53.0	121.5 ± 53.5
LV end-diastolic volume index, mL/m^2	67.8 ± 13.3	81.5 ± 16.9	79.7 ± 19.0
LV end-systolic volume, mL	47.5 ± 18.7	63.4 ± 31.0	61.7 ± 29.7
LV end-systolic volume index, mL/m^2	25.5 ± 8.7	39.5 ± 11.3	40.2 ± 11.4
LV mass, g	126.2 ± 36	97.6 ± 46	90.4 ± 46
LV mass index, g/m^2	67.9 ± 14.8	60.3 ± 14.2	57.8 ± 14.0
LV mass-to-volume ratio, g/mL	1.02 ± 0.22	0.75 ± 0.18	0.74 ± 0.18
LV ejection fraction, %	63 ± 7	52 ± 7	50 ± 5
RV end-diastolic volume, mL	-	-	202.9 ± 79
RV end-diastolic volume index, mL/m^2	-	-	135.0 ± 33
RV end-systolic volume, mL	-	-	103.7 ± 44
RV end-systolic volume index, mL/m^2	-	-	68.1 ± 17
RV ejection fraction, %	-	-	49 ± 8
Pulmonary regurgitant fraction, %	-	-	37 ± 18

*Subjects with repaired TOF with serial CMR data.
†Age calculated from twenty-six out of ninety-nine subjects with available data.
Values provided are taken from the first CMR examination.
Values are shown as count (%), mean $\pm$ SD, or *n*, unless otherwise indicated.
TOF is tetralogy of Fallot; BSA, body surface area; LV, left ventricle; RV, right ventricle; EF, ejection fraction.

Table 2.2. Summary of differences in LV and RV measurements between the baseline and follow-up CMR examinations.

Variable	Mean Difference ± SD	Median Difference (Range)
Age, y	2.8 ± 1.6	2.1 (1.1 - 7)
LV end-diastolic volume index, mL/m^2	4.9 ± 7.8	4.6 (-8.8 - 19.1)
LV end-systolic volume index, mL/m^2	3.7 ± 9.7	4.1 (-11.6 - 23.3)
LV mass index, g/m2	6.2 ± 10.9	4.1 (-10.7 - 25.6)
LV mass-to-volume ratio, g/mL	0.028 ± 0.15	-0.010 (-0.28 - 0.34)
LVEF, %	-0.2 ± 7.5	0.1 (-15 - 16)
RV end-diastolic volume index, mL/m^2	7.5 ± 23.4	3.0 (-25 - 71)
RV LV end-systolic volume index, mL/m^2	4.6 ± 14.0	0.3 (-16 - 41)
RVEF, %	-0.7 ± 4.3	-0.7 (-14.6 - 5.3)
Pulmonary regurgitant fraction, %	-0.4 ± 6.3	0.2 (-20.5 - 5.4)

LV, left ventricle; RV, right ventricle; EF, ejection fraction; SD, standard deviation

Table 2.3. Differences in CMR parameters between subjects with an increase or decrease in ejection fraction over the follow-up duration.

	First CMR examination			Second CMR examination			Difference		
	Positive ΔLVEF	Negative ΔLVEF	p-value	Positive ΔLVEF	Negative ΔLVEF	p-value	Positive ΔLVEF	Negative ΔLVEF	p-value
Age, y	20.6 ± 10	17.8 ± 15	0.62	23.2 ± 11	20.7 ± 15	0.67	2.6 ± 2	2.9 ± 2	0.74
LVEDVi, mL/m^2	79.4 ± 15	80.0 ± 23	0.95	80.8 ± 11	88.4 ± 20	0.31	1.4 ± 7	8.5 ± 7	**0.04**
LVESVi, mL/m^2	41.6 ± 9	38.9 ± 13	0.61	37.8 ± 8	50.2 ± 17	0.05	-3.8 ± 5	11.3 ± 7	**<0.001**
LV mass index, g/m^2	58.6 ± 9	57.0 ± 18	0.81	63.8 ± 11	64.3 ± 17	0.94	5.2 ± 9	7.3 ± 13	0.68
LV mass/volume, g/mL	0.77 ± 0.2	0.72 ± 0.1	0.57	0.80 ± 0.1	0.74 ± 0.2	0.44	0.03 ± 0.2	0.02 ± 0.2	0.92
LVEF, %	48 ± 6	52 ± 4	0.10	54 ± 6	46 ± 7	**0.03**	6 ± 5	-6 ± 5	**<0.001**
RVEDVi, mL/m^2	136.8 ± 34	133.2 ± 33	0.82	142.8 ± 39	142.2 ± 32	0.97	6.1 ± 18	8.9 ± 29	0.79
RVESVi, mL/m^2	68.6 ± 19	67.7 ± 15	0.91	72.8 ± 21	72.6 ± 15	0.98	4.2 ± 16	4.9 ± 13	0.91
RVEF, %	50 ± 10	49 ± 5	0.79	49 ± 7	49 ± 5	0.95	-1 ± 6	0 ± 2	0.70
PR fraction, %	37.3 ± 17	40.5 ± 18	0.70	37.8 ± 20	39.1 ± 18	0.89	0.5 ± 5	-1.4 ± 7	0.51

Values are shown as mean ± standard deviation. Significant p-values are shown in bold.

LV, left ventricle; RV, right ventricle; EDVi, end-diastolic volume index; ESVi, end-systolic volume index; PR, pulmonary regurgitant; EF, ejection fraction

Table 2.4. Correlation of standard and novel parameters at baseline with changes in global measures of left ventricular volume and mass.

Response variable (difference over time)	Best baseline standard predictor	R^2	Adj. R^2	p-value	Best baseline shape atlas predictor	R^2	Adj. R^2	p-value
LVEDVi	LVEDVi	0.32	0.189	0.099	Reference mode 9	0.16	0.007	0.401
LVESVi	LVEF	0.21	0.057	0.285	**TOF mode 8**	**0.40**	**0.289**	**0.038**
LV mass index	LV mass index	0.30	0.166	0.121	TOF mode 5	0.24	0.102	0.204
LV mass/volume	**LV mass/volume**	**0.39**	**0.273**	**0.045**	TOF mode 5	0.36	0.238	0.063
LVEF	LVEF	0.20	0.045	0.309	**TOF mode 7**	**0.46**	**0.358**	**0.018**

Multiple regression models controlled for the age at baseline CMR examination and follow-up duration. Statistically significant baseline predictor variables are in bold ($p<0.05$)

TOF is tetralogy of Fallot; EDVi, end-diastolic volume index; ESVi, end-systolic volume index; EF, ejection fraction; ED, end-diastolic; .
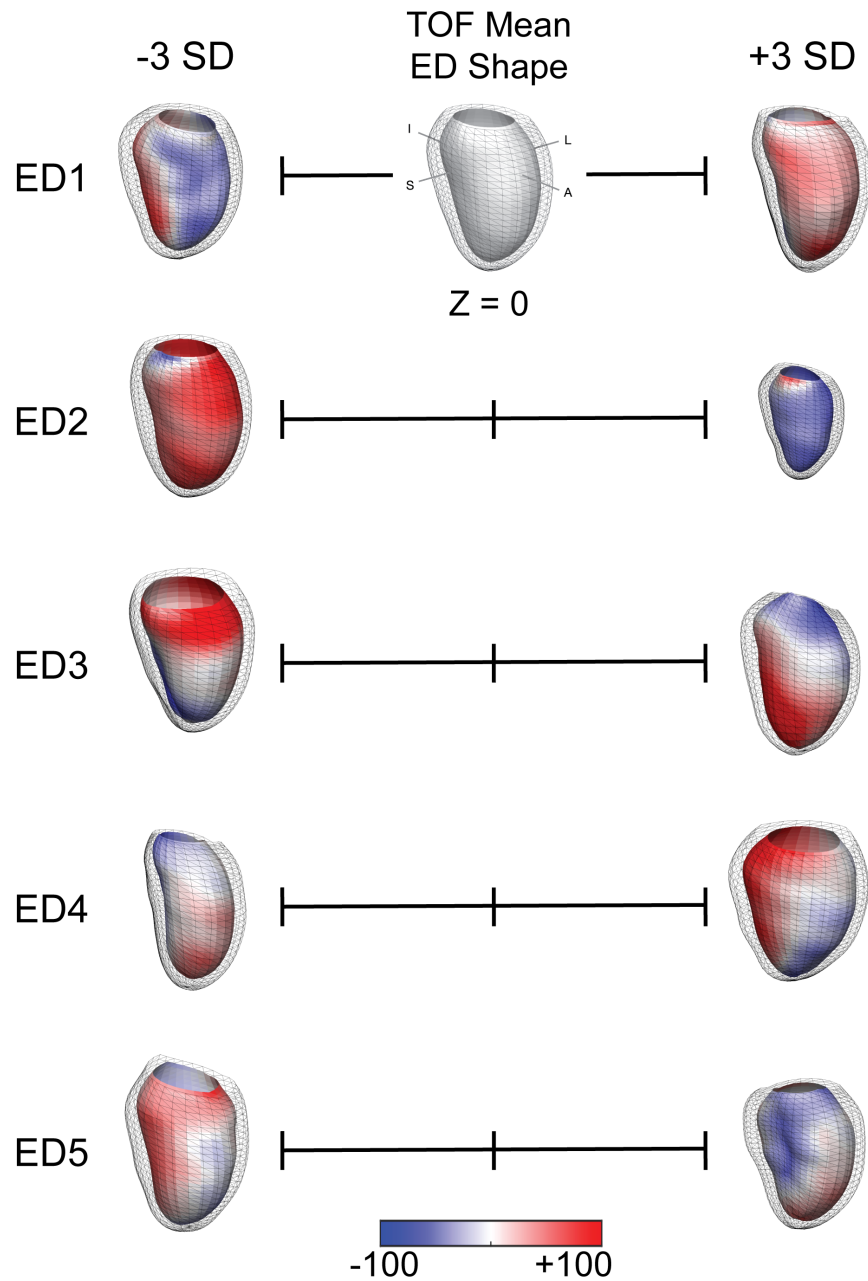
Figure 2.1. Statistical variation of the top-ranked modes of the TOF atlas of LV end-diastolic shape. Color indicates the percentage difference in regional wall volume relative to the TOF mean. LV orientation indicated by anatomical axis labels: septal (S), lateral (L), anterior (A), and inferior (I). TOF is tetralogy of Fallot; ED, end-diastole; SD, standard deviation.
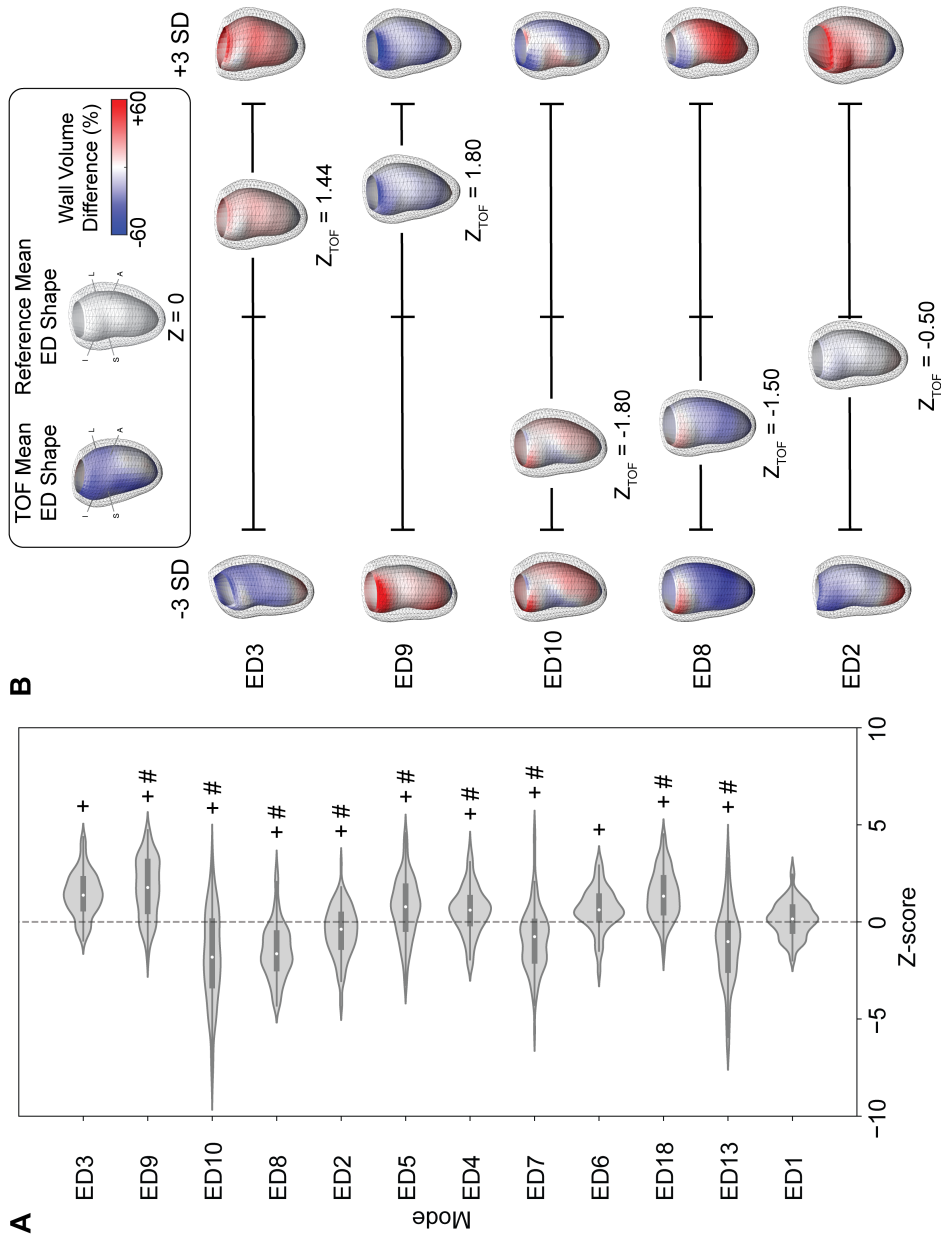
Figure 2.2. Comparison of subjects with repaired TOF to the reference atlas of LV end-diastolic shape. A) Distribution of ED shape mode Z-scores represented as kernel density estimates and boxplots. Symbols represent a significant difference in mean ($^{+}p < 0.01$) or variance ($^{\#}p < 0.01$) relative to the normal reference population with correction for multiple comparisons. B) ED shape and wall volume variation for the five modes of the reference atlas that account for the largest difference of subjects with TOF. Each row shows the left ventricular shape for each mode from a Z-score of -3 to +3 in units of SD, relative to the reference mean (Z-score = 0), as well as the shape corresponding to the mean Z-score for TOF subjects (Z_T-OF). Variation in wall volume, shown as color on the endocardial surface, is represented as the difference in regional wall volume relative to the mean of normal subjects. Orientation of the left ventricle indicated by anatomical axes: anterior (A), inferior (I), septal (S), and lateral (L). TOF is tetralogy of Fallot; SD, standard deviation; ED, end-diastolic.
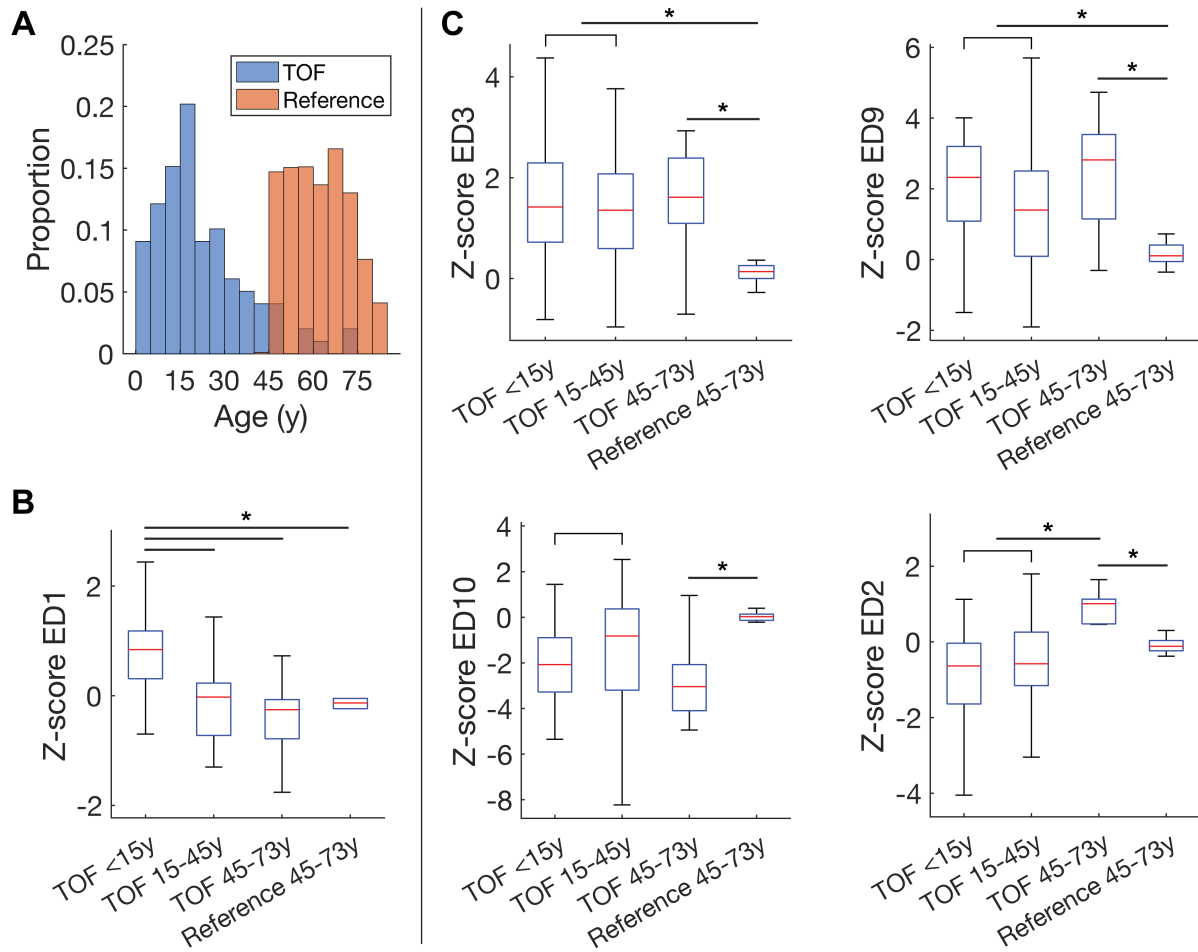
Figure 2.3. Age-related differences in LV end-diastolic shapes. A) Distribution of ages in the TOF and reference groups. Distributions of shape mode Z-scores by age groups for modes of the reference atlas reflecting B) overall LV size and C) modes that accounted for the largest proportion of difference between the TOF and reference groups. Lines indicate significant differences in mode scores between groups ($p < 0.05$). TOF is tetralogy of Fallot; ED, end-diastolic.
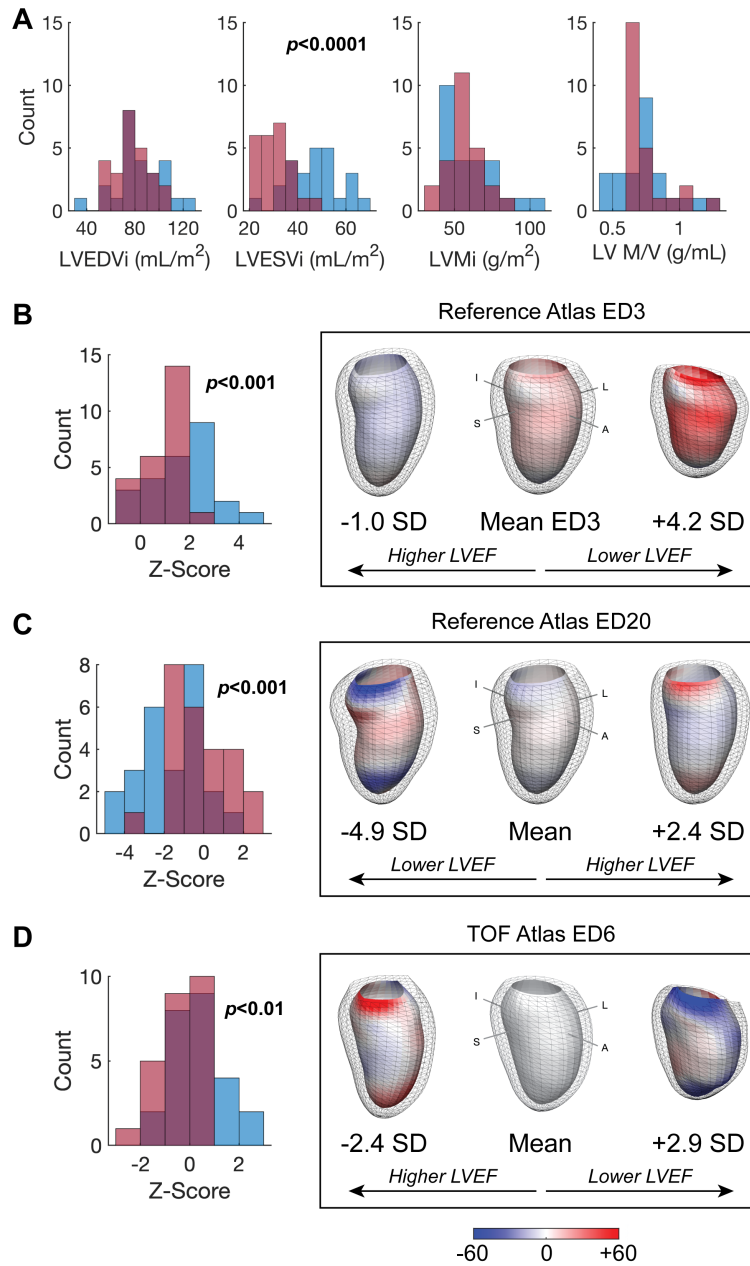
Figure 2.4. Association of parameters of end-diastolic shape to left ventricular ejection fraction for subjects with repaired TOF. A) Distributions of standard indexed CMR parameters of remodeling and B-D) shape mode Z-scores for high (red bars) and low (blue bars) LVEF groups. *P*-values correspond to differences in group means between subjects below the 25th (lower quartile, Q1) and above the 75th (upper quartile, Q3) percentiles of LVEF. Shape and regional wall volume representations of ED modes that are associated with LVEF show the mean and range of shape for subjects with TOF. Arrows indicate direction of shape variation associated with a high or low LVEF in TOF subjects. Colors indicate the percentage difference in wall volume from the mean LV shape. Orientation of LV indicated by anatomical axes: septal (S), lateral (L), anterior (A), and inferior (I). ED is end-diastolic; LVEF, left ventricular ejection fraction; EDVi, end-diastolic volume index; ESVi, end-systolic volume index; Mi, mass index; M/V, mass-to-volume ratio; and SD, standard deviation.

52
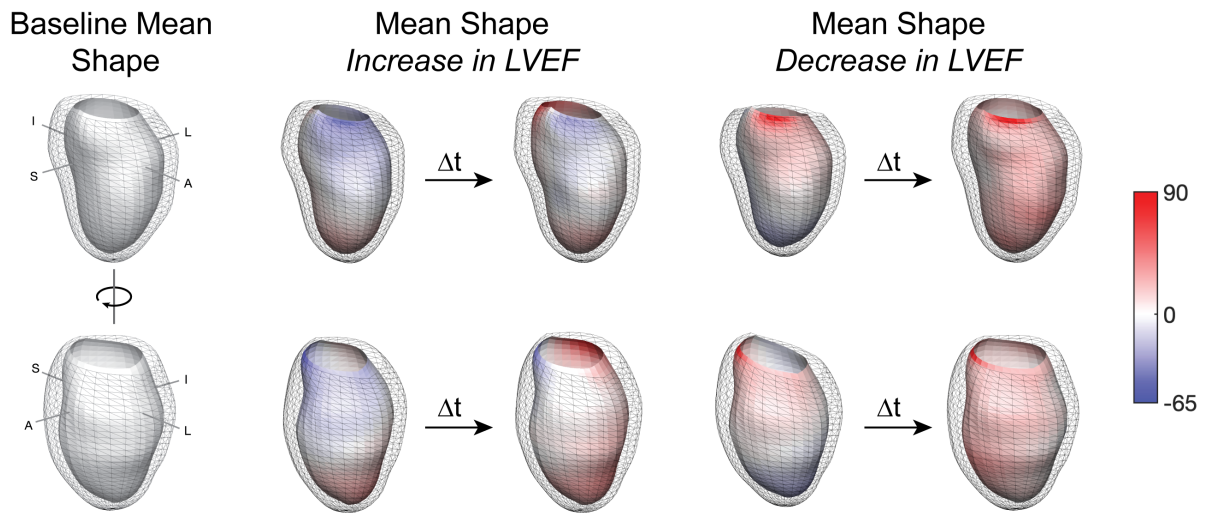
Figure 2.5. Shape and wall volume differences between subjects with an increase or decrease in ejection fraction over time. Colors denote the percentage difference in wall volume from the mean shape at baseline. Anatomical orientation of each row indicated by the baseline mean shape: septal (S), lateral (L), anterior (A), and inferior (I). LVEF, left ventricular ejection fraction; Δt, time between the first and second CMR examination.
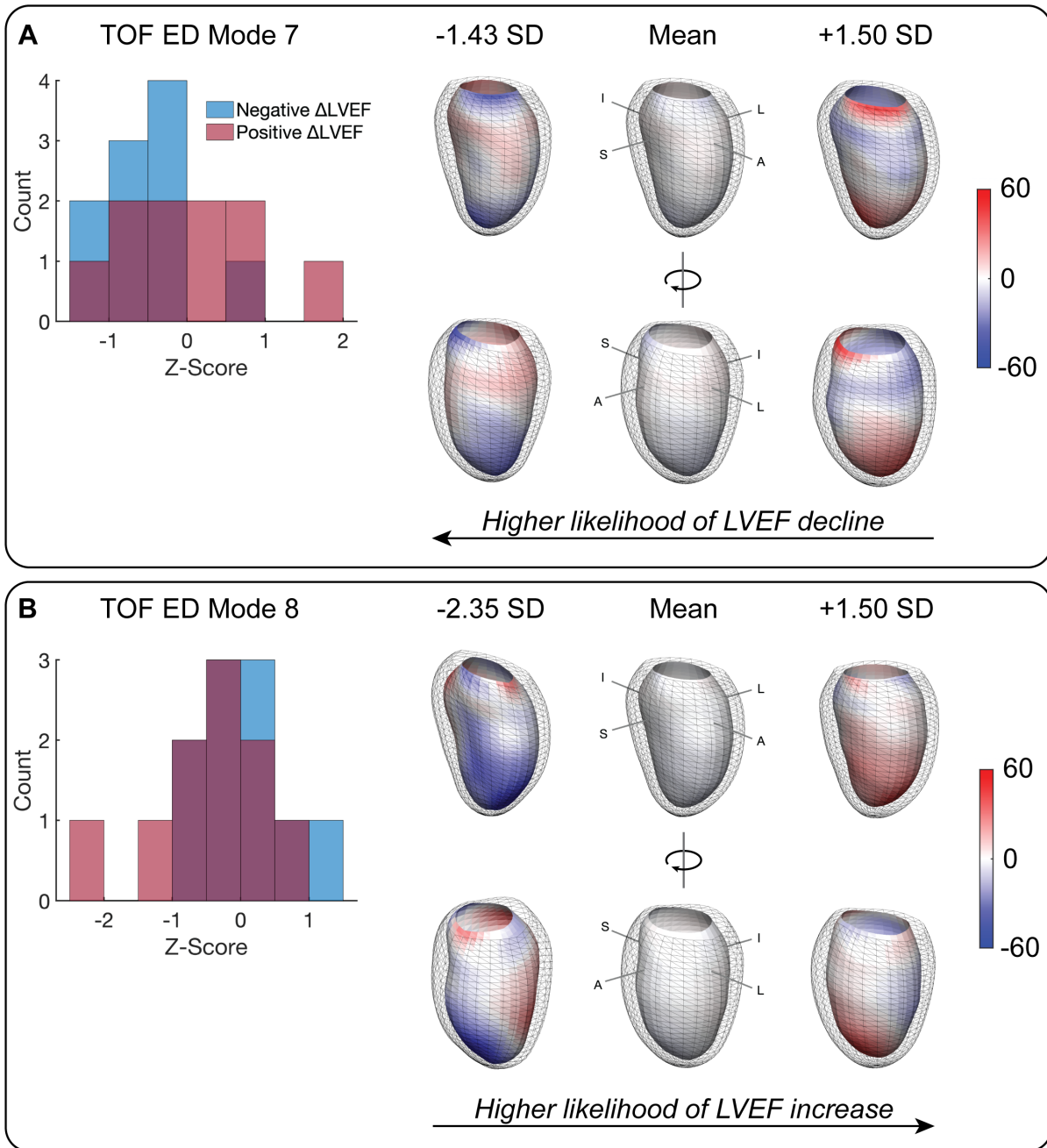
Figure 2.6. Statistical variation of end-diastolic shapes that best predicted the change in global systolic function. Mode score distributions and representations of shape and wall volume for A) TOF atlas A) mode 7 and B) mode 8. The shape corresponding to the minimum, mean, and maximum Z-score for each mode is represented. Wall volume difference projected on the endocardial surface is relative to the mean shape (center). Orientation of LV indicated by anatomical axes: septal (S), lateral (L), anterior (A), and inferior (I). TOF, tetralogy of Fallot; LVEF, left ventricular ejection fraction; SD, standard deviation

Chapter 3

Morphological Markers and Determinants of Left Ventricular Systolic Dysfunction in Repaired Tetralogy of Fallot

3.1 Abstract

Patients with repaired tetralogy of Fallot (TOF) are at risk of long-term left ventricular (LV) dysfunction with associated poor outcomes. While adverse inter-ventricular interactions in the presence of right ventricular volume overload and dyssynchrony have been implicated, morphological remodeling of the LV may contribute to LV systolic dysfunction. In this study, we examined the association of LV end-diastolic (ED) shape with components of systolic wall motion (SWM) that contribute to global systolic dysfunction. Features of LV shape associated with sphericity, wall thickness, and valve plane orientation correlated with components of SWM. The effect of ED shape perturbations on SWM were examined in a finite element analysis of systolic ventricular mechanics. The combination of ED shape and myocardial contractility were able to explain and match predicted measures of SWM. From the results of this study, we hypothesize that greater LV conicity, a tilted valve plane orientation, and a flatter septal wall are markers of reduced myocardial contractility and should be examined further for clinical prognostic utility to improve patient outcomes.

3.2   Introduction

Despite a clinical focus on preserving right ventricular (RV) structure and function, patients with repaired tetralogy of Fallot (TOF) are at risk of developing left ventricular (LV) systolic dysfunction in the long term. LV dysfunction is prevalent in 20% of patients with repaired TOF and has been linked to risk of heart failure and mortality [52]. Improvements in surgical strategy to preserve the pulmonary valve and prevent the detrimental effects of pulmonary regurgitation have been shown to reduce RV dysfunction and interventricular dyssynchrony; however, this strategy potentially leads to reduced LV longitudinal shortening and LV intraventricular dyssynchrony [84]. Patients are also at risk of adverse morphological remodeling of the LV, and this may worsen global systolic function. There exists a clear need to better understand the mechanisms of LV dysfunction in order to better evaluate, predict, and prevent poor long-term outcomes.

Cardiac magnetic resonance (CMR) imaging is considered the gold standard for quantitative assessment of cardiac structure and function, but conventional strategies do not take full advantage of the four-dimensional (4D) information in a single dataset. Standard assessment relies on measurements derived from a priori knowledge of cardiac anatomy and function, but patient prognosis remains limited and much of the information in a CMR dataset is underutilized. Better assessment of the complex features of LV systolic function has the potential to discover important patterns with mechanistic insight that are otherwise hidden. Additionally, computational modeling of cardiac mechanics has the ability to test various mechanisms of pathophysiology in repaired TOF.

In this study, we used a large, cross-sectional cohort of subjects with repaired TOF to identify end-diastolic (ED) shape features that correlated with components of systolic dysfunction. We tested for the mechanistic dependency of systolic function on targeted shape features using finite element models of LV mechanics with the goal of identifying shape determinants and markers of myocardial dysfunction.

3.3   Methods

3.3.1   Subjects and Data Collection

This study analyzed retrospective CMR datasets from subjects with repaired tetralogy of Fallot acquired for clinical purposes at Rady Children's Hospital San Diego (San Diego, California, USA) and the Centre for Advanced MRI (Auckland, New Zealand). All images and data were obtained as part of the Cardia Atlas Project (CAP) and used in accordance with local institutional review boards (IRB) at the University of California, San Diego ("The Cardiac Atlas Project", La Jolla, California, USA) and the University of Auckland (Auckland, New Zealand) [44]. Data from a reference population comprising 1,991 asymptomatic adults with anatomically normal hearts were used for comparison [26]. Clinically acquired LV pressure data from intracardiac catheterization were obtained and de-identified for a portion of study subjects from medical records associated with CMR datasets.

3.3.2   Cardiac MR Image Acquisition

Images used in this study were acquired using 1.5 T magnetic resonance imaging scanners, including Phillips Intera (Phillips Healthcare, Best, The Netherlands), Siemens Avanto (Siemens Medical Systems, Erlangen, Germany), and GE Discovery and Signa (GE Healthcare, Milwaukee, USA). Each subject underwent standard functional CMR examination within the scope of clinical practice. Two-dimensional cine images used in this study were acquired using steady state free precession imaging and were prospectively or retrospectively gated with acquisition of at least thirty reconstructed phases per RR interval. Short axis slices spanning from the base to the apex were acquired. At least two long-axis imaging planes (two-chamber, four-chamber, or LV outflow tract) were acquired through valve annuli.

3.3.3 Atlas-Based Analysis of Systolic Wall Motion

This study used a statistical atlas of systolic wall motion (SWM) derived from the reference population to quantify SWM in the TOF group. The atlas of SWM was derived from principal component analysis (PCA) of a set of 1,991 models of three-dimensional (3D) ED and ES shape. Briefly, SWM was calculated as the displacement of 3D points from ED to ES (ES - ED). The set of displacements for all cases were combined into an N by P matrix as input to the PCA algorithm for N cases and P points per case. PCA extracted 1,990 orthogonal components, or "modes", of SWM ranked by the amount of variance explained by each mode.

Individual models of SWM were generated for each subject using a guide-point modeling process. Guide-point modeling involves fitting a 3D template model to a set of short and long axis CMR images by aligning to anatomical landmarks of the mitral valve and insertion points of the RV free wall at the interventricular septum. The model is fit to subject-specific ventricular geometry by least-squares optimization in a semi-automated process that relies on a combination of automated contour edge detection and manually placed guide-points defined by the analyst. Fitted shape models at ED and ES are sampled at the endocardial and epicardial surfaces and scaled according to subject height. For each case, the set of sampled points were projected onto the reference atlas of SWM to calculate subject-specific Z-scores for each mode.

3.3.4 Sensitivity of Global Function to Components of Systolic Wall Motion

The effect of atlas modes of SWM on global systolic function was analyzed by varying individual modes and computing the resulting LV ejection fraction (EF). For each mode of SWM, wall motion displacements, D_i, for altered mode score i were generated and added to the mean ED shape of TOF subjects to calculate the resulting ES shape, S_i^{ES} (Equation 3.1). ED and ES model volumes, V_i, were used to calculate EF_i (Equation 3.2).

$$S_i^{ES} = \mu^{ED} + D_i \tag{3.1}$$

$$EF_i = \frac{(V_i^{ED} - V_i^{ES})}{V_i^{ED}} \qquad (3.2)$$

3.3.5 Correlation Between Left Ventricular Shape and Systolic Wall Motion

This study tested for correlations between atlas modes of ED shape with modes of SWM. ED shape modes were part of an atlas of LV ED shape derived from the same population of reference subjects used for the SWM atlas. Pearson correlation analysis was used to test for significant correlations between Z-scores of ED shape and SWM. Multivariate linear regression analysis was used to assess the correlation between an ED shape mode and a set of SWM modes.

3.3.6 Finite Element Analysis of Left Ventricular Systolic Mechanics

Finite element (FE) analysis was used to test for the mechanistic dependency of SWM on ED geometries of the TOF group. An overview of the process for running a FE simulation of systolic mechanics for various ED geometries is shown in Figure 3.1. A cubic-Hermite FE mesh template was fit to a unique set of 3D coordinate points from the LV ED shape atlas for each tested geometry. An incompressible, nonlinearly elastic material model was used to define the passive constitutive properties of the myocardium (Holzapfel and Ogden 2009).This constitutive model uses a structurally based definition of material properties in the fiber, sheet, and cross-fiber directions. Mesh fiber directions were assigned using a rule-based approximation, which were defined as -60 degrees relative to the circumferential direction of the LV at the epicardium and +60 degrees at the endocardium. Fiber directions varied linearly from the epicardium to the endocardium to define a physiologically realistic transmural gradient. Systolic myocardial dynamics were modeled using a time-varying elastance framework where active force is generated using a length-dependent activation model. An iterative algorithm was used to approximate the unloaded, stress-free geometry as in Krishnamurthy et al. [57]. The unloaded geometry approximation was validated by calculating the root mean square (RMS) error

between the fitted ED geometry and the geometry of the unloaded mesh inflated to ED pressure. Nodal boundary conditions were implemented to constrain the longitudinal and circumferential displacement of the epicardium at the base. Additionally, a pressure boundary condition was applied normal to the endocardial surface. Pressure was modeled as a linear increase from ED pressure to ES pressure based on intracardiac pressures estimated from TOF subjects with available data.

Passive material properties for the average TOF subject were approximated by first estimating the unloaded volume, V_0, using the Klotz empirical formula for estimation of the ED pressure-volume relationship [85]:

$$V_0 = V_{ED}(0.6 - 0.006 * P_{ED}) \qquad (3.3)$$

Values from average human were used for six out of the eight material constants (b, a_s, b_s, b_f, a_{fs}, and b_{fs}). The remaining constants, a and a_f, were estimated by altering these parameters until the unloaded volume was achieved in the unloaded geometry approximation. The material anisotropy ratio of a to a_f was maintained so that only a single parameter was estimated. Active material properties were approximated by altering parameter T_{active}^{max} – the peak active tension generated – until the mean ES volume was reached after contraction of the mean ED model.

Additional FE simulations were repeated with perturbations of ED geometry corresponding to the 5th and 95th percentile Z-score of tested shape modes. For each model, the same active and passive material parameters estimated for the base model representing the TOF average were used. The endocardial and epicardial surfaces of the initial and deformed mesh geometry were sampled in order to calculate wall motion displacements. The resulting sampled displacements were projected onto the atlas of SWM to compute Z-scores for each mode. SWM Z-scores from FE model simulations were compared with those predicted from linear regression models fit to subject data.

3.3.7 Statistical Analysis

Mean scores of SWM modes between the TOF and reference groups were tested for differences using an unpaired t-test; if group variances were not assumed to be equal, a Welch's unpaired t-test was used. Statistical analysis was performed using the SciPy Python library (https://www.scipy.org). Statistical significance was evaluated at the 0.05 level. For repeated tests, a *post hoc* Holm-Bonferroni correction was used to adjust the significance level and correct for the likelihood of making a Type I error.

3.4 Results

3.4.1 Reference Atlas of Systolic Wall Motion

The variation in the first five modes of the reference atlas of SWM and the mean for TOF subjects are shown in Figure 3.2. These modes explain over 70% of variation in the reference population. Qualitatively, the first mode (SWM1) represents variation in longitudinal wall motion; the second mode (SWM2) represents variation in wall thickening; the third mode (SWM3) represents variation in the deviation of the valve plane normal; the fourth mode (SWM4) represents variation in the radial and longitudinal wall motion, with an inverse relationship between wall thickening and longitudinal shortening; and the fifth mode (SWM5) represents variation in the degree of valve plane widening or narrowing.

3.4.2 Analysis of Systolic Function in TOF

This study used a TOF cohort of ninety-nine subjects used in a prior study (median age, age range). The mean LVEF was 52%, and global systolic dysfunction (LVEF $< 55\%$) was present in 66% of subjects. The most abnormal modes of SWM are shown in Figure 3.3. Across the TOF cohort, nine out of the ten most abnormal modes had a significant difference in mean compared to the asymptomatic reference population (Figure 3.3A). Primary SWM abnormalities were reduced longitudinal and radial wall motion, and diminished radial wall motion of the

septal wall.

The association of modes of SWM with LVEF are shown in Figure 3.4. LVEF was most sensitive to SWM modes 2 through 7. For the average TOF subject, the largest contributors to diminished LVEF were modes 2, 3, and 4, in order. These same modes correlated with several modes of ED shape from the reference ED atlas (Figure 3.5). Multivariate regression analysis revealed ED modes 3, 5, 2, and 9 were most strongly correlated with SWM, in order. The strongest correlation was between ED mode 2, representing variation in apical wall mass, septal wall morphology, and valve plane orientation, and SWM mode 3, representing variation in valve plane motion (r = -0.45, $p < 0.0001$). In summary, features of LV shape related to conicity, basal wall mass, and valve plane diameter correlated with the wall thickening mode of SWM (SWM2). Features of LV sphericity and valve plane orientation correlated with systolic deviation of the valve plane normal and longitudinal shortening (SWM3 and SWM4).

3.4.3   Analysis of Systolic Wall Motion Using Finite-Element Analysis

A summary of the accuracy of the FE model for the TOF mean is shown in Figure 3.6. Parameterization of the material properties of the base model resulted in a root mean square error (RMSE) of 3.39 mm between the inflated unloaded geometry (simulated ED shape) compared to the mean ED shape derived from the data (Table 3.2). The deformed mesh from the mechanics model was analyzed after optimization of the active contractility of the base model to achieve the target EF of 52%. The resulting SWM Z-scores of the simulated model were calculated and compared to the mean SWM of the data for the four SWM modes of interest (Figure 3.6). The largest difference in Z-score was for SWM mode 2, with a Z-score difference of 0.67.

The perturbed ED shapes and their resulting deformed ES shape from FE simulations are shown in Figure 3.7. For several modes, shape perturbation resulted in a marked deviation of LVEF from the mean of the base model (Table 3.2). LVEF was most sensitive to variations of ED shape modes 5 and 9. Increasing the Z-score to the 95th percentile shape for ED mode 5, which decreased the valve plane diameter and apical wall mass, resulted in a lower LVEF. Similarly,

for ED mode 9, a lower LVEF resulted from altering shape to the 95th percentile Z-score, i.e., greater LV conicity and a more pointed apex resulted in a lower LVEF.

Comparison of the resulting SWM due to variation of ED shape with that predicted from significant correlations in the data are shown in Figure 3.8. The closest agreement between data and simulation was found for the relationship between SWM mode 3 and ED mode 3. The slope of the simulated relationship was 0.16 compared to 0.28 in the data. Simulated SWM Z-scores were outside of the 95% confidence interval of the predicted values for the 5th percentile and mean ED shape for ED3, but within the error of the predicted value for the 95th percentile shape. For the relationship between SWM mode 2 and ED mode 5 from the FE model, the sign of the slope was opposite to the regression model from the data but matched the predicted SWW mode 2 Z-score for the 5th percentile shape. For ED mode 2 versus SWM mode 3, only the 5th percentile of ED mode 2 matched the predicted Z-score of the regression model.

For FE models that did not match the predicted SWM, the contractility parameter was adjusted until the SWM was within the 95% confidence interval of the predicted value. The direction of shape mode variation that associated with lower contractility is indicated in Figure 3.9. For ED mode 2, greater apical wall mass, reduced infero-septal wall mass, flatter septal wall, and a more lateral facing valve plane were associated with lower contractility (Figure 3.9B). For ED mode 3, greater sphericity, rounder apex, greater overall wall mass, and more lateral facing valve plane were associated with lower contractility (Figure 3.9C). For ED mode 5, greater conicity, greater basal wall mass, and larger valve plane diameter were associated with lower contractility (Figure 3.9D).

3.5   Discussion

Patients with repaired TOF are at risk of developing LV dysfunction despite being burdened by a primarily right-sided disease. In this study, we sought to determine the effect of LV morphology on systolic mechanics by systematically altering ED geometry in models

of FE mechanics. Abnormal features of ED shape were significantly correlated with modes of SWM from a reference atlas of asymptomatic adults that were the largest contributors to global dysfunction. In simulations of systolic mechanics, variations in ED geometry partially explained variation in SWM. Modification of model contractility was able to adjust resultant components of SWM to match predictions from TOF subject data. ED shapes that were more abnormal relative to the reference population mean were associated with lower contractility. Specifically, greater overall conicity, a rounder apex, a flatter septal wall morphology, and a tilted valve plane orientation were associated with lower contractility. Altogether, these results present features of LV shape which are determinants of systolic dysfunction and potential markers of impaired myocardial contractility. Routine clinical assessment of patients with repaired TOF may benefit from an atlas-based analysis of shape and function to improve patient prognosis.

3.5.1 Determinants of Left Ventricular Dysfunction in Repaired TOF

We compared our cohort of TOF subjects to a reference population of asymptomatic adults to quantify abnormal components of SWM. We found that the most significant contributors to global dysfunction in TOF were components of SWM related to wall thickening, transverse basal motion, and, to a lesser extent, longitudinal shortening. Several studies have demonstrated decreased radial, circumferential, and longitudinal deformation in TOF [86, 87, 63, 80, 88, 84, 64, 60, 89]. Furthermore, CMR analysis has identified myocardial deformation parameters that relate to symptoms and clinical deterioration in patients with repaired TOF, and are strongly associated with long-term outcomes [64, 63]. Routine clinical assessment of ventricular dysfunction, especially of the LV, is an important strategy as mortality and morbidity typically depend on LV function [54, 66, 90, 65].

Possible causes of LV dysfunction could be related to electromechanical dyssynchrony, abnormal septal defects and motion, and altered hemodynamic preload or afterload in the presence of moderate to severe pulmonary regurgitation. Studies of LV dysfunction and dyssynchrony have shown a link to QRS duration, septal curvature, and RV function and dilation

64

[90, 87, 89, 61, 80, 60]. Few studies have associated systolic function with complex measures of ventricular morphology beyond traditional patterns of remodeling that are based on indexed ED mass and relative wall thickness [17, 91, 92]. We found significant correlations between modes of ED shape and modes of SWM in our cohort of TOF subjects: features of LV shape related to conicity, basal wall mass, and valve plane diameter correlated with the wall thickening mode; features of LV sphericity and valve plane orientation correlated with systolic deviation of the valve plane normal and longitudinal shortening.

Much of the analysis of LV dysfunction in TOF is focused on adverse interactions with the RV, since there exists a well-studied correlation between LV and RV ejection fraction. However, there is little knowledge about the coupled effect of RV dysfunction on long-term LV remodeling and function. MRI-based studies showed that reduced RV EF due to severe PR is linked to a reduced LV EF [91, 93]. Additionally, ventricular fibrosis and pulmonary regurgitation are known to cause adverse remodeling, and have been related to LV and RV dysfunction in repaired TOF [94, 93]. Generally, these studies lack insights into the mechanisms of ventricular coupling. Here, we sought to discover measurable factors associated with LV dysfunction as well as determinants of dysfunction that are significantly altered in repaired TOF.

In our FE analysis of systolic mechanics, we found variations in ED shape features related to the length-to-width ratio and valve plane orientation (ED2 and ED3) were capable of partially explaining the relationship between these shape modes and modes of SWM. However, the resultant model SWM did not match values predicted from correlations in the data for all tested shape variations. For example, altering ED mode 3 resulted in a sensitivity slope of 0.16 for SWM mode 3, while linear regression of the subject-specific scores predicted a slope of 0.28. Modification of model contractility was able to correct the relationship between ED mode 3 and SWM mode 3 (Figure 3.9C). This suggests that approximately 60% of variation in SWM mode 3 can be attributed to variation in ED mode 3, while the rest is potentially attributable to altered passive and active material properties. We found altered contractility to be a likely factor since changing it in the model resulted in more accurate systolic deformations. In our FE

analysis of ED mode 5 and SWM mode 2, we found a positive correlation that was opposite to that predicted by data, i.e., greater conicity and a larger valve plane diameter correlated with greater wall thickening (Figure 3.9D). This result suggests shape features associated with ED mode 5 may reflect a compensatory remodeling mechanism to preserve systolic function in the presence of adverse passive or active myocardial properties.

3.5.2   Limitations

Analysis of systolic wall motion was limited to radial, circumferential, and longitudinal components since our shape modeling process does not track material point displacements. As a result, we were unable to assess torsional components of LV function. In the future, this can be addressed by modifying shape modeling software to be compatible with tagged magnetic resonance imaging datasets, for example. Furthermore, the shape model template used to fit to the unique geometry of each subject was based on normal LV anatomy and shape. Use of a template that is based on the complex ventricular anatomy specific to TOF may be better at capturing important regions of shape variation, and warrants further investigation.

The finite element models used in our analysis of systolic mechanics used several simplifications. Namely, material properties were assumed to be homogeneous throughout the myocardium, rather than incorporating regional heterogeneities that might be present due to scarring or fibrosis. Additionally, myocardial fiber architecture was simplified as a linear transmural gradient, rather than using more realistic properties. This was primarily due to the lack of fiber property data in repaired TOF. We also prescribed a simple hemodynamic pressure boundary condition, rather than using a closed-loop, lumped parameter circulatory model. However, as we were only concerned with measuring deformed mesh geometry at ES, a complex circulatory model was not necessary for our analysis. Finally, our models did not incorporate boundary conditions related to interactions with the RV, pericardium, atria, or any fluid-structure interactions. Further effort should be made towards developing methods for statistical and mechanical analysis of biventricular geometries, potentially incorporating a full,

four-chamber anatomy.

3.5.3   Conclusions

Using a novel framework that incorporated statistical atlas data with computational models of systolic mechanics, this study demonstrated the dependence of LV systolic function on ED shape in a cohort of repaired TOF. Significant correlations between highly abnormal features of ED shape and components of systolic wall motion were discovered and examined using FE models of systolic mechanics. Wall motion components related to wall thickening and tilting of the valve plane were sensitive to variations in ED sphericity, conicity, wall mass near the base, and valve plane diameter. Adjustment of myocardial contractility was sufficient to match predicted SWM to ED shape, identifying shape markers which associated with altered contractility. Markers of shape and function from statistical atlases have the potential to provide more precise indicators of adverse remodeling in repaired TOF and can be more closely examined through models incorporating detailed mechanisms of pathophysiology.

3.6   Acknowledgements

Chapter 3, in full, is material in preparation to be submitted for publication: N. Forsch, S. Salehyar, K. Gilbert, A. Suinesiaputra, S. Hegde, J.C. Perry, A.A. Young, J.H. Omens, and A.D. McCulloch. Morphological Markers and Determinants of Left Ventricular Systolic Dysfunction in Repaired Tetralogy of Fallot. The dissertation author is the first author of this article.

Table 3.1. Summary of finite element model properties

Model Component	Specifications
Element Mesh	Cubic Hermite elements ED geometry from inflated unloaded geometry estimation
Passive material model	Nonlinearly elastic orthotropic model with fiber, sheet, and cross-fiber parameters [95]
Active model	Time-varying, length-dependent active tension
Boundary conditions	Linearly increasing endocardial pressure Longitudinal and circumferential baseplane displacement constraints

Table 3.2. Finite element model geometries tested in simulations of systolic mechanics

Model	End-diastolic geometry	End-diastolic mesh RMS error (mm)	Ejection fraction (%)
0	Mean of TOF	3.39	52%
1	ED mode 2 Z = -2.91	4.24	50.1%
2	ED mode 2 Z = 1.41	3.01	51.7%
3	ED mode 3 Z = -0.40	3.90	51.5%
4	ED mode 3 Z = 3.53	3.13	49.8%
5	ED mode 5 Z = -2.01	2.27	54.6%
6	ED mode 5 Z = 2.20	4.28	48.2%
7	ED mode 9 Z = -0.80	2.81	54.5%
8	ED mode 9 Z = 4.40	4.23	44.3%
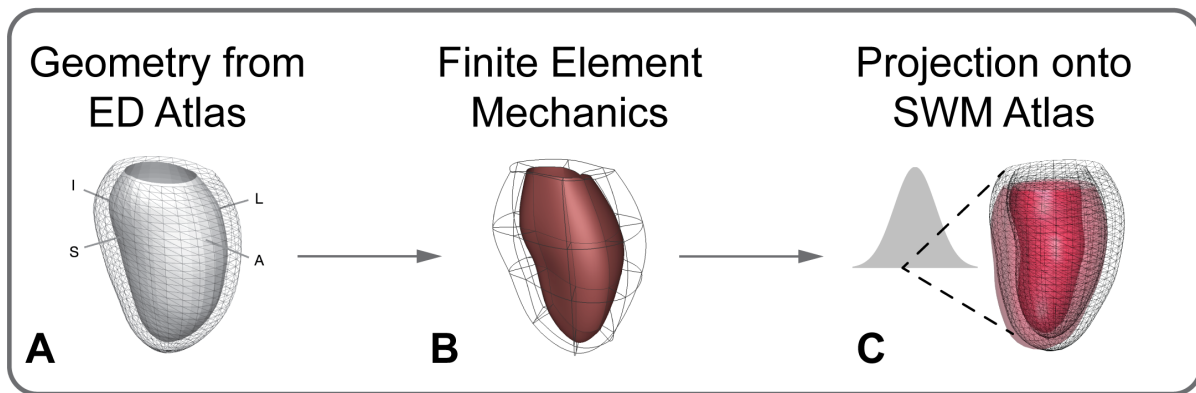
Figure 3.1. Process of simulating left ventricular mechanics from atlas geometries. A) Geometries from the statistical distribution of an end-diastolic shape atlas are varied in a finite element analysis framework. B) Deformed end-systolic meshes from models of mechanics are extracted and C) projected into an atlas of systolic wall motion to compute resulting Z-scores for each case. This process is repeated for each model perturbation. ED is end-diastolic; SWM, systolic wall motion.
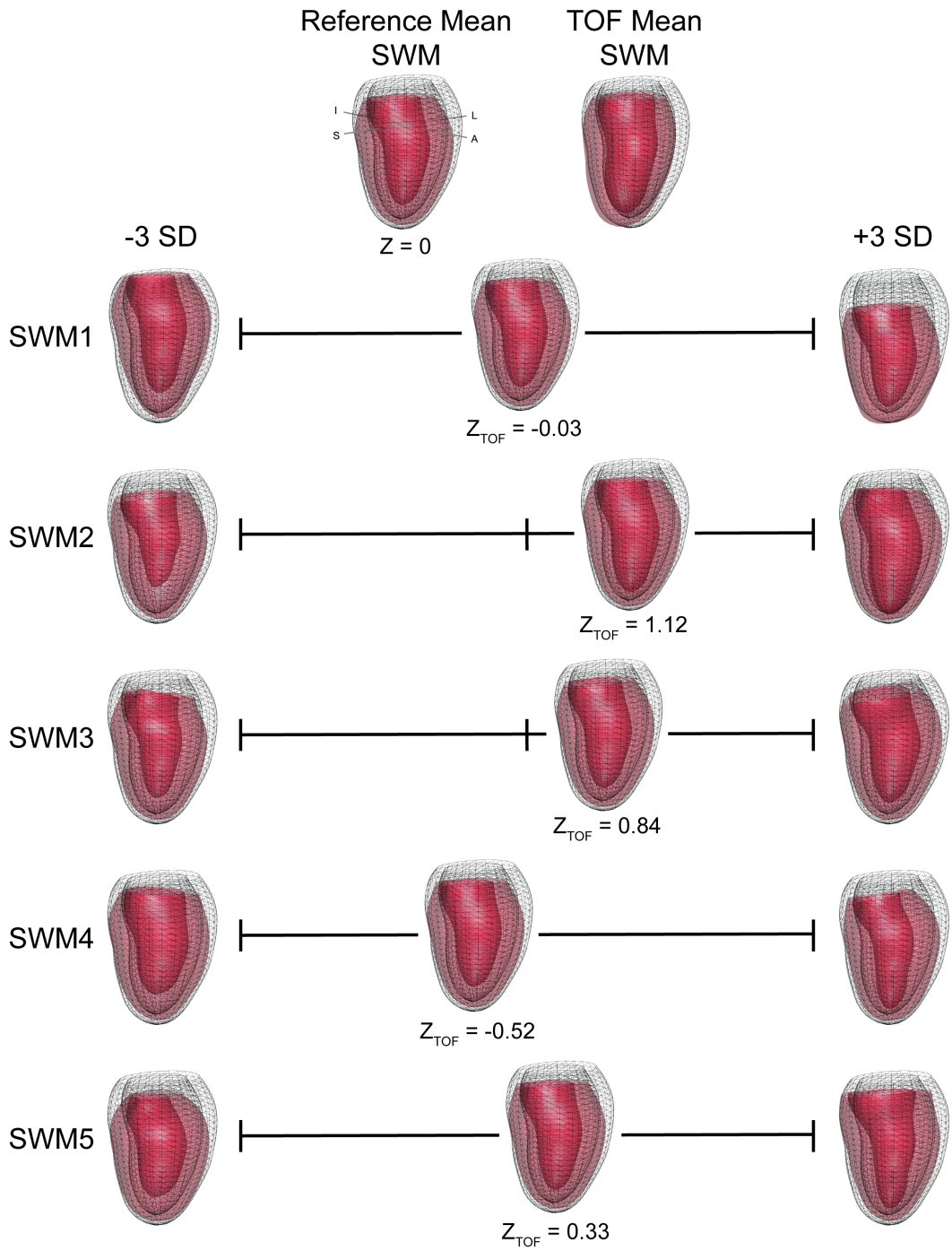
Figure 3.2. Top-ranked PCA modes of systolic wall motion of the reference population showing the mean of the TOF group. Systolic wall motion is represented as an overlay of end-systolic shape (red) on the mean end-diastolic shape (black wireframe). The mean TOF systolic wall motion for each mode is shown between the variation of -3 to +3 SD relative to the reference mean. SWM is systolic wall motion; TOF, tetralogy of Fallot; SD, standard deviation.
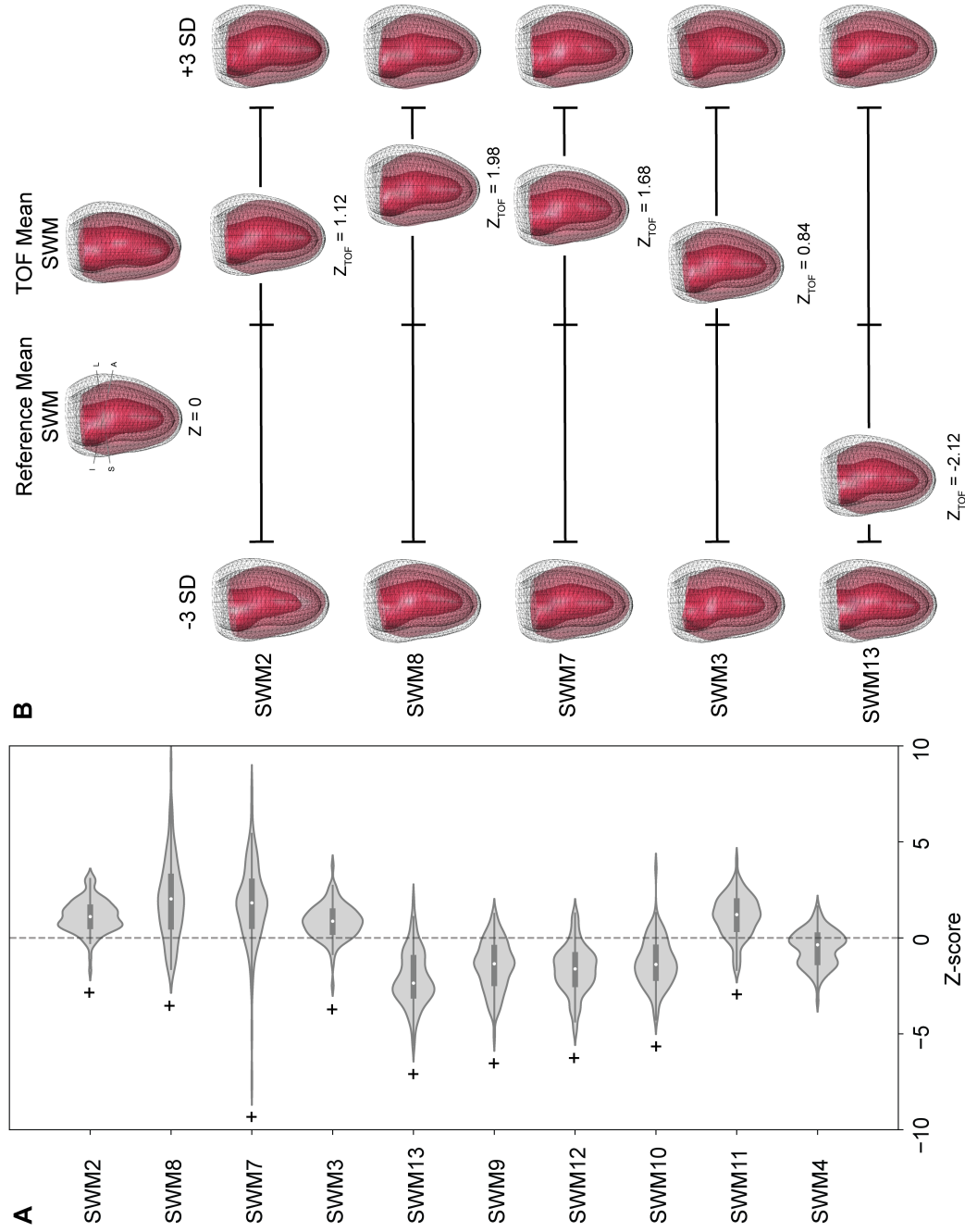
Figure 3.3. Abnormalities of systolic wall motion in the repaired TOF cohort. A) Boxplot with kernel density estimates and B) 3D depictions of modes of systolic wall motion ranked by the fraction of mean difference from the reference population. Symbols indicate a significant difference in systolic wall motion mode Z-score means ($^+ p <$0.05). 3D depictions are shown as a range of variation from -3 to +3 SD relative to the reference mean (ED in black; ES in red). SWM is systolic wall motion; ED, end-diastolic; ES, end-systolic; TOF, tetralogy of Fallot; SD, standard deviation.
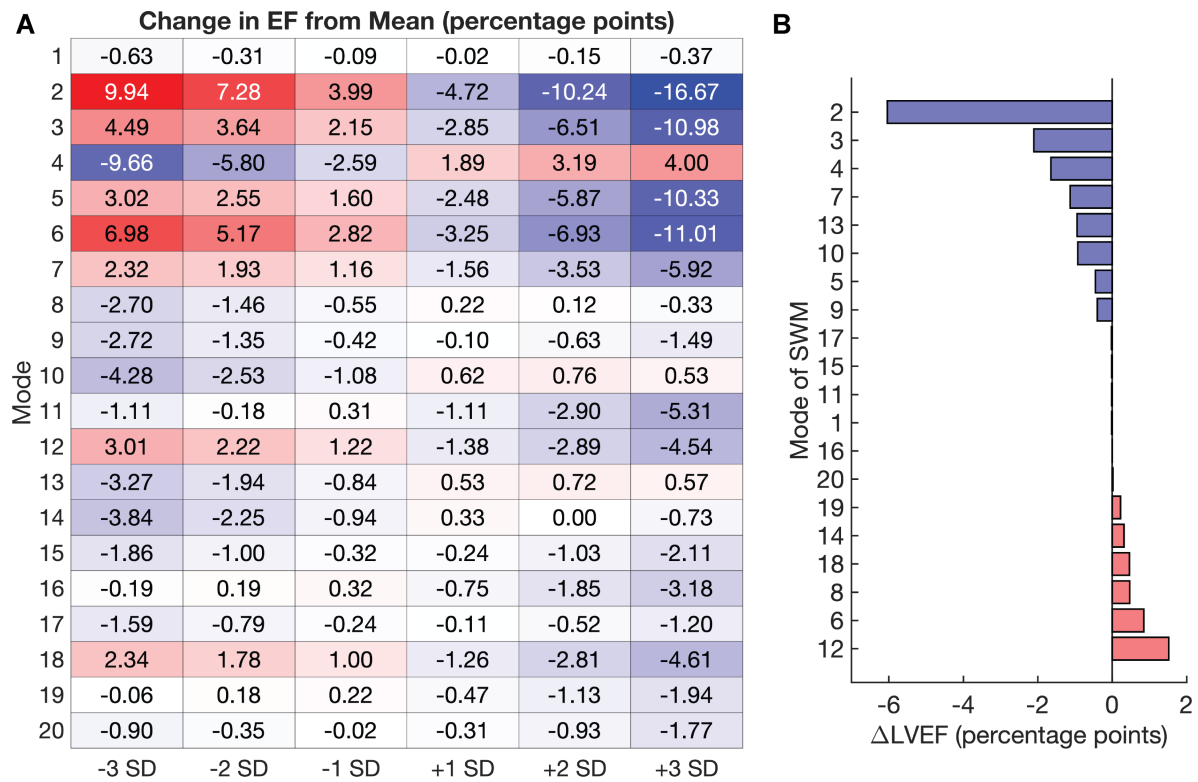
Figure 3.4. Association of systolic wall motion modes with LV ejection fraction. A) Difference in LV ejection fraction from the mean for variations in modes of systolic wall motion. Positive values indicate gain of function (red) and negative values indicate loss of function (blue). B) Estimated net effect of modes of systolic wall motion on LV ejection fraction for the average TOF subject. Modes are ranked from most negative to most positive effect on LVEF. SWM is systolic wall motion; EF, ejection fraction

	Pearson r			R^2
	2	3	4	[2,3,4]
3	0.13	0.36*	0.33*	0.29*
5	-0.39*	0.25	-0.13	0.23*
2	-0.08	-0.45*	0.21	0.23*
9	0.35*	0.00	-0.09	0.13
10	-0.29	-0.21	0.13	0.13
20	-0.02	-0.35*	0.01	0.13
7	0.13	-0.16	0.25	0.10
1	0.27	0.07	-0.12	0.09
14	0.26	0.00	0.08	0.07
4	-0.10	-0.02	0.25	0.07
17	0.09	-0.14	0.19	0.06
11	-0.06	-0.13	-0.17	0.06

Mode of ED Shape (vertical axis) / Mode of SWM (horizontal axis)

Figure 3.5. Correlation of modes of systolic wall motion with modes of end-diastolic shape. Heatmap indicates the multivariate correlation R^2 value for each end-diastolic mode with the set of systolic wall motion modes 2, 3, and 4, as well as Pearson r correlation coefficients between individual modes. End-diastolic shape modes are ranked by overall correlation with the set of systolic wall motion modes. Symbols indicate statistically significant correlations ($^*p <0.05$). SWM is systolic wall motion; ED, end-diastolic.
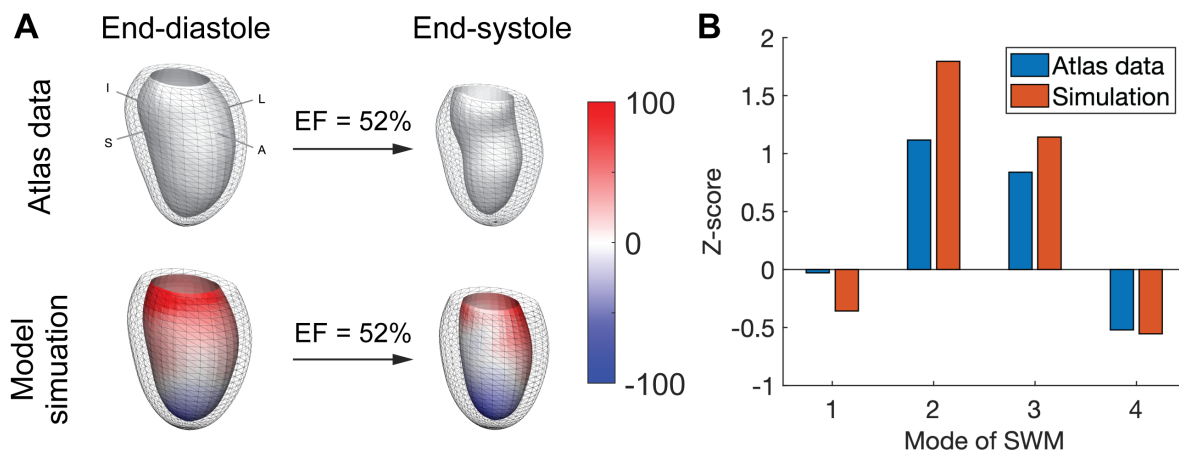
Figure 3.6. Accuracy of the base finite element model relative to data. A) The mean end-diastolic and end-systolic shapes of the TOF cohort are shown next to shapes of the simulated base model. Color indicates percentage wall volume difference of the simulated model relative to the data. B) Comparison of the resulting systolic wall motion mode Z-scores of the simulated model versus the data for the TOF mean. ED is end-diastolic; ES, end-systolic; SWM, systolic wall motion; EF, ejection fraction.

5th percentile of ED mode

ED_model   ES_model

95th percentile of ED mode

ED_model   ES_model

ED mode 2

Z_{ED2} = -2.91   EF = 50.1% Z_{ED2} = 1.41   EF = 51.7%

ED mode 3

Z_{ED3} = -0.40   EF = 51.5% Z_{ED3} = 3.53   EF = 49.8%

ED mode 5

Z_{ED5} = -2.01   EF = 54.6% Z_{ED5} = 2.20   EF = 48.2%

ED mode 9

Z_{ED9} = -0.80   EF = 54.5% Z_{ED9} = 4.40   EF = 44.3%
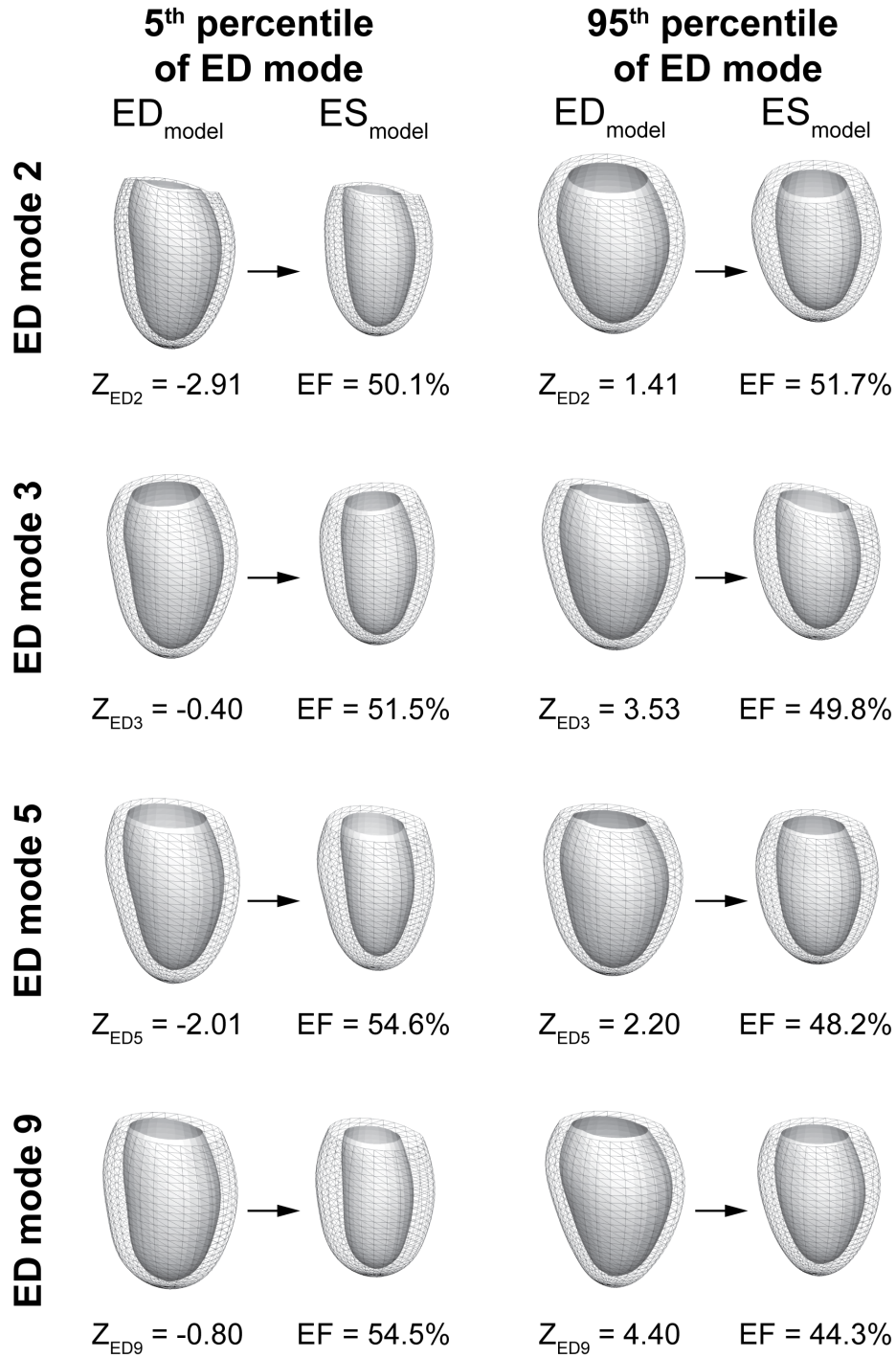
Figure 3.7. End-diastolic perturbations and resulting deformed end-systolic shape for finite element models. The end-diastolic shape of the finite element model is shown next to the resulting simulated end-systolic shape of the model. Models are oriented with the antero-septal wall towards the front. ED is end-diastolic; ES, end-systolic; EF, ejection fraction.
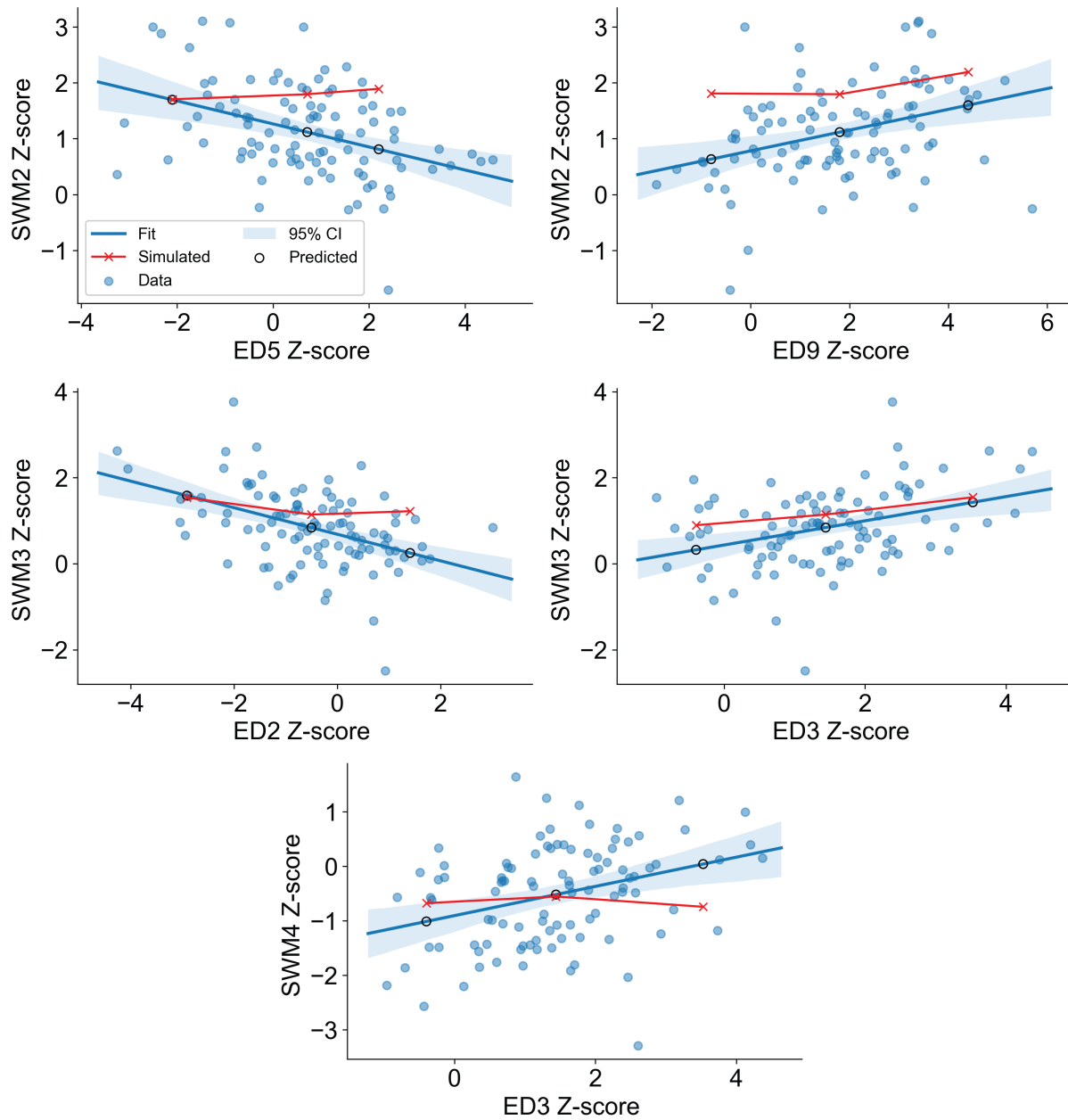
Figure 3.8. Comparison of predicted and simulated systolic wall motion due to end-diastolic shape perturbations. Significant correlations from TOF subject data between modes of end-diastolic shape and modes of systolic wall motion are represented as combined scatterplots and linear regression models with 95% confidence intervals. ED is end-diastolic; SWM, systolic wall motion; CI, confidence interval.
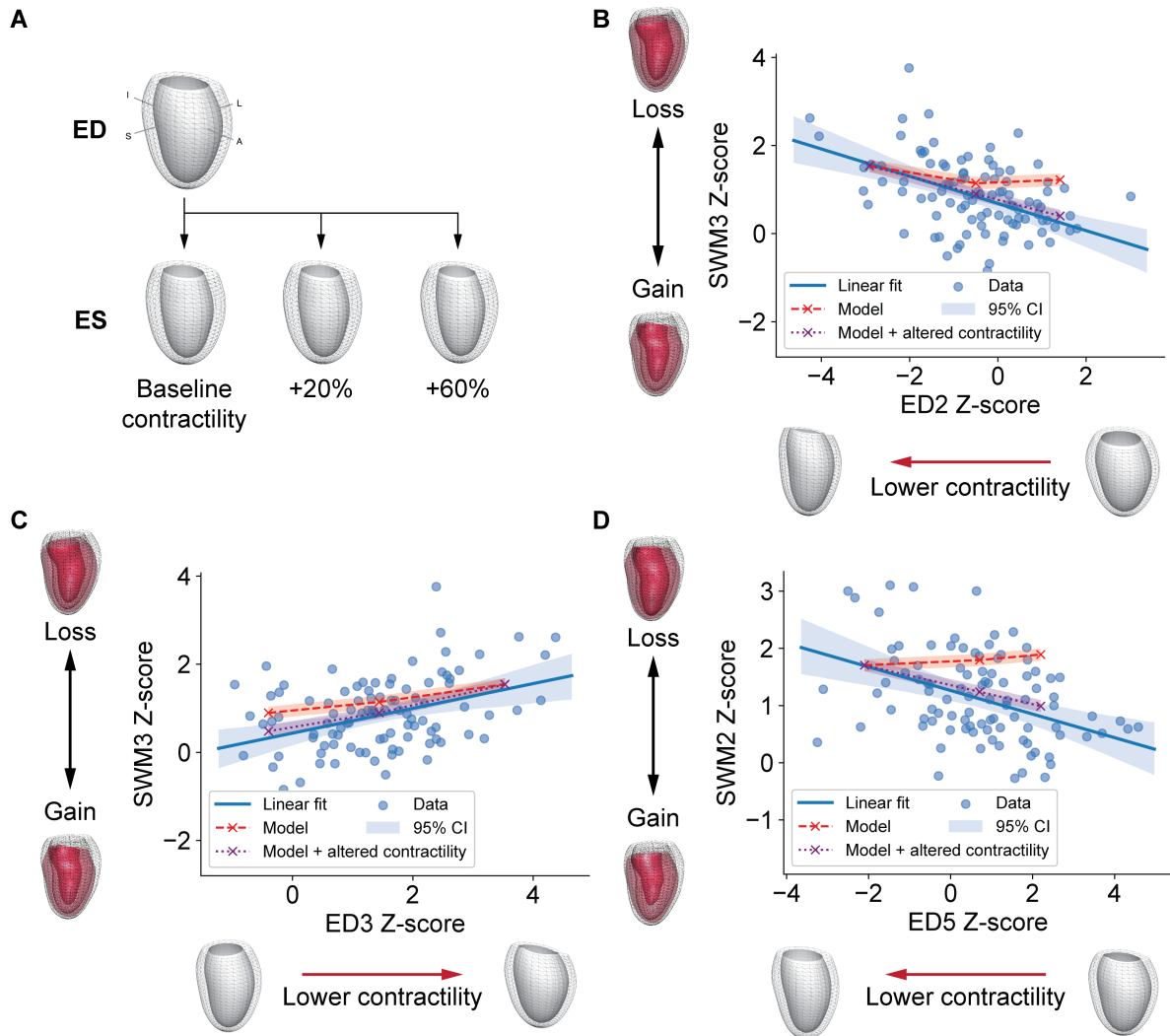
Figure 3.9. Correction of resultant systolic wall motion by alteration of myocardial contractility. A) Demonstration of the effect of altered contractility on end-systolic geometry. B-D) Changes in systolic wall motion due to altered contractility indicating the direction of ED shape mode variation associated with lower model contractility. Model line shading represents the error in calculation of SWM Z-scores. Representative variation of systolic wall motion is shown alongside the y-axis. Orientation of the LV indicated by anatomical axis labels: septal (S), lateral (L), anterior (A), and inferior (I). ED is end-diastole; ES, end-systole; SWM, systolic wall motion; CI, confidence interval.

Chapter 4

Conclusion of the Dissertation

We have successfully demonstrated the use of statistical shape atlases for the characterization of left ventricular (LV) morphology and systolic function in repaired tetralogy of Fallot (TOF) to gain new insights into disease markers and mechanisms of adverse LV remodeling.

In Chapter 1, we derived an atlas of LV end-diastolic (ED) shape from ninety-nine patients to qualitatively and quantitatively describe the statistical variation within this cohort. We used guide-point modeling techniques to capture the three-dimensional (3D) LV shape using cardiac magnetic resonance (CMR) image data and applied dimensionality reduction techniques to extract orthogonal modes of LV shape variation and compute patient-specific metrics. We tested whether novel shape atlas markers would have clinical prognostic relevance by correlating baseline measures of shape with changes in LV function over time in a small patient sub-cohort and found a significant correlation between a TOF atlas shape mode and the change in LV ejection fraction. We also outlined the process of using models of finite element mechanics to examine associations of ED shape patterns with systolic function. The findings in this chapter present the first use of a statistical shape atlas of the LV in this clinical population. By taking full advantage of the 3D data contained in cardiac magnetic resonance (CMR) image data, the TOF LV atlas can better characterize variations in LV shape than standard CMR assessment. When tested alongside standard clinical indices of LV remodeling in a small study, shape atlas features more strongly associated with a measure of LV deterioration, demonstrating the potential to

supplement clinical prognostic assessment.

Next, we expanded our analysis of LV morphology in repaired TOF by comparing patients with an atlas derived from an asymptomatic reference population (Chapter 2). The reference atlas revealed highly significant abnormalities but was unable to explain a large portion of shape variation in TOF. We discovered modes of ED shape from both atlases that were associated with global systolic function. Furthermore, in a test cohort of twenty patients, we found that the best correlate with the change in LV ejection fraction (EF) were modes of ED shape from the TOF atlas, rather than a mode of shape from the asymptomatic reference atlas or a standard clinical index of remodeling. These significant features represented variations in LV conicity, apex morphology, and antero-septal wall curvature, which may contain mechanistic insight. Taken together, the results of this chapter compare and validate the use of distinct statistical LV atlases for a comprehensive assessment of a TOF patient group. A reference atlas of normal cardiac anatomy derived from a population free of known cardiovascular disease can inform adverse remodeling with functional consequences across many cardiovascular disease types. However, for prognostic purposes, shape features derived from the atlas of the congenital group were the only measures to associate with LV deterioration. This discovery suggests that standard CMR assessment and statistical features of shape variation from asymptomatic populations may be insufficient for monitoring disease progression in a patient cohort.

Based on associations between shape and LVEF that we observed, we used an atlas of systolic wall motion to identify components of function which were the largest contributors to diminished LVEF in repaired TOF. We found significant correlations between ED shape and systolic wall motion that we tested in a finite element analysis framework. We measured a partial dependence of systolic function on ED shape and hypothesized that several shape features were markers of impaired myocardial contractility. These findings are a demonstration of the convergence and co-utility of statistical and mechanistic modeling approaches for elucidation of disease mechanisms. In the presence of measurement error and uncertainty, mechanistic models can be parameterized based on the statistical variation of a population to determine

pathophysiological mechanisms of a clinical group such as TOF without needing to rely on patient-specific measurements. Additionally, mechanistic model frameworks can leverage atlases of cardiac physiology (e.g., shape, electrical activation, and fiber architecture) to assess model sensitivity to parameters based on the variation measured in a population.

Future work can address several issues with atlas construction from clinical image data, as outlined in the chapters above. Methods would benefit from the use of data from other imaging modalities, such as 2D or 3D echocardiography, as this data can be more easily acquired in clinical practice. Furthermore, atlas-based analyses would benefit from more standardized intervals of imaging in congenital heart disease (CHD) patients, to minimize the heterogeneity of data and to better assess long-term changes. The process of atlas construction can leverage advanced machine learning techniques to automate image segmentation and patient-specific model generation. Indeed, collaborators involved with this work are developing novel methods to train machine learning algorithms on the complex anatomy of various forms of CHD.

The hypothesis that shape atlas modes measured and presented in this dissertation are markers of myocardial contractility can be further tested with more detailed computational models of finite element mechanics. These models should incorporate biventricular anatomy to observe and measure the impact of the right ventricle on LV systolic mechanics and include more realistic boundary conditions to more accurately match measured myocardial deformations. In general, we found the reported literature on myocardial fiber architecture in TOF to be lacking, highlighting the need for a more rigorous and comprehensive analysis of this property. Additionally, models should incorporate regional heterogenities in passive and contractile material properties to account for scarring and akinetic regions of the myocardium as these may account for dysfunction measured in patients.

Finally, continuous effort should be made to aggregate additional CMR and associated clinical data and increase the sample size of statistical atlases in order to better represent the variability of the TOF population. The differences observed in the TOF group presented in this thesis my be attributable to other patient factors, including diagnoses and clinical sub-

types, the surgical approach used for repair, interventions such as pulmonary valve replacement or systemic artery-to-pulmonary artery shunt, gender, genetics, and co-morbidities. Atlases can be constructed of subclinical populations, such as of TOF patients with pulmonary valve replacement or of patients with different forms of surgical repair, once enough data is collected and analyzed. The results of Chapter 2 should be validated in a large, independent test cohort of patients once sufficient additional data is made available.

As shown by the work in this dissertation, quantitative assessment of LV morphology and function by utilizing statistical cardiac atlases has the potential to supplement clinical decision support by identifying more specific markers of adverse remodeling. This approach can help generate hypotheses of the physiological mechanisms of remodeling and holds great promise as a valuable clinical tool to assist cardiologists and other healthcare practitioners in delivering personalized care for the individual patient.

Bibliography

[1] E. Fallot, Contribution a l'anatomie pathologique de la maladie bleu (cyanose cardiaque), Marseille méd 25 (1888) 77–138.

[2] D. van der Linde, E. Konings, M. Slager, M. Witsenburg, W. Helbing, J. Takkenberg, J. Roos-Hesselink, Birth prevalence of congenital heart disease worldwide: a systematic review and meta-analysis, Journal of the American College of Cardiology 58 (21) (2011) 2241–2247.

[3] T. Geva, B. M. Sandweiss, K. Gauvreau, J. E. Lock, A. J. Powell, Factors associated with impaired clinical status in long-term survivors of tetralogy of fallot repair evaluated by magnetic resonance imaging, J Am Coll Cardiol 43 (6) (2004) 1068–1074.

[4] E. Bradley, J. Parker, E. Novak, P. Ludbrook, J. Billadello, A. Cedars, Cardiovascular disease in late survivors of tetralogy of fallot: a tertiary care center experience, Texas Heart Institute Journal 40 (4) (2013) 418.

[5] P. Davlouros, P. Kilner, T. Hornung, W. Li, J. Francis, J. Moon, G. Smith, T. Tat, D. Pennell, M. Gatzoulis, Right ventricular function in adults with repaired tetralogy of fallot assessed with cardiovascular magnetic resonance imaging: detrimental role of right ventricular outflow aneurysms or akinesia and adverse right-to-left ventricular interaction, Journal of the American College of Cardiology 40 (11) (2002) 2044–2052.

[6] M. K. Friedberg, A. N. Redington, Right versus left ventricular failure: differences, similarities, and interactions, Circulation 129 (9) (2014) 1033–1044.

[7] P. Lurz, R. Puranik, J. Nordmeyer, V. Muthurangu, M. S. Hansen, S. Schievano, J. Marek, P. Bonhoeffer, A. M. Taylor, Improvement in left ventricular filling properties after relief of right ventricle to pulmonary artery conduit obstruction: contribution of septal motion and interventricular mechanical delay, Eur Heart J 30 (18) (2009) 2266–2274.

[8] D. Tobler, A. M. Crean, A. N. Redington, G. S. Van Arsdell, C. A. Caldarone, K. Nanthakumar, D. Stambach, L. Dos, B. J. Wintersperger, E. N. Oechslin, et al., The left heart after pulmonary valve replacement in adults late after tetralogy of fallot repair, Int J Cardiol 160 (3) (2012) 165–170.

[9] C. A. Smith, C. McCracken, A. S. Thomas, L. G. Spector, J. D. St Louis, M. E. Oster, J. H. Moller, L. Kochilas, Long-term outcomes of tetralogy of fallot: A study from the pediatric cardiac care consortium, JAMA Cardiol 4 (2019) 34–41.

[10] J. Therrien, G. R. Marx, M. A. Gatzoulis, Late problems in tetralogy of fallot - recognition, management, and prevention, Cardiol Clin (2002).

[11] S. V. Babu-Narayan, G. P. Diller, R. R. Gheta, A. J. Bastin, T. Karonis, W. Li, D. J. Pennell, H. Uemura, B. Sethia, M. A. Gatzoulis, D. F. Shore, Clinical outcomes of surgical pulmonary valve replacement after repair of tetralogy of Fallot and potential prognostic value of preoperative cardiopulmonary exercise testing, Circulation 129 (1) (2014) 18–27.

[12] A. Frigiola, M. Hughes, M. Turner, A. Taylor, J. Marek, A. Giardini, T. Y. Hsia, K. Bull, Physiological and phenotypic characteristics of late survivors of tetralogy of Fallot repair who are free from pulmonary valve replacement, Circulation 128 (17) (2013) 1861–1868.

[13] A. S. Rotes, B. W. Eidem, H. M. Connolly, C. R. Bonnichsen, J. K. Rosedahl, H. V. Schaff, J. A. Dearani, H. M. Burkhart, Long-term follow-up after pulmonary valve replacement in repaired tetralogy of Fallot, Am J Cardiol 114 (6) (2014) 901–908.

[14] D. Yim, L. Mertens, C. T. Morgan, M. K. Friedberg, L. Grosse-Wortmann, A. Dragulescu, Impact of surgical pulmonary valve replacement on ventricular mechanics in children with repaired tetralogy of fallot, Int J Cardiovasc Imaging 33 (2017) 711–720.

[15] T. Geva, Repaired tetralogy of fallot: the roles of cardiovascular magnetic resonance in evaluating pathophysiology and for pulmonary valve replacement decision support, J Cardiovasc Magn Reson 13 (1) (2011) 9.

[16] T. Geva, Indications and timing of pulmonary valve replacement after tetralogy of fallot repair, Pediatr Card Surg Annu 9 (2006) 11–22.

[17] M. G. Khouri, R. M. Peshock, C. R. Ayers, J. A. de Lemos, M. H. Drazner, A 4-tiered classification of left ventricular hypertrophy based on left ventricular geometry, Circ Cardiovasc Imaging 3 (2010) 164–171.

[18] R. J. Van Der Geest, J. H. Reiber, Quantification in cardiac MRI, J Magn Reson Imaging 10 (5) (1999) 602–608.

[19] A. A. Young, B. R. Cowan, S. F. Thrupp, W. J. Hedley, L. J. Dell'Italia, Left ventricular mass and volume: Fast calculation with guide-point modeling on MR images, Radiology 216 (2000) 597–602.

[20] C. Chen, C. Qin, H. Qiu, G. Tarroni, J. Duan, W. Bai, D. Rueckert, Deep learning for cardiac image segmentation: A review, Front Cardiovasc Med 7 (2020) 25.

[21] A. N. Bhuva, W. Bai, C. Lau, R. H. Davies, Y. Ye, H. Bulluck, E. McAlindon, V. Culotta, P. P. Swoboda, G. Captur, T. A. Treibel, J. B. Augusto, K. D. Knott, A. Seraphim, G. D. Cole, S. E. Petersen, N. C. Edwards, J. P. Greenwood, C. Bucciarelli-Ducci, A. D. Hughes, D. Rueckert, J. C. Moon, C. H. Manisty, A multicenter, scan-rescan, human and machine learning cmr study to test generalizability and precision in imaging biomarker analysis, Circ Cardiovasc Imaging 12 (2019).

[22] M. R. Avendi, A. Kheradvar, H. Jafarkhani, Automatic segmentation of the right ventricle from cardiac MRI using a learning-based approach, Magn Reson Med 78 (2017) 2439–2448.

[23] W. Bai, M. Sinclair, G. Tarroni, O. Oktay, M. Rajchl, G. Vaillant, A. M. Lee, N. Aung, E. Lukaschuk, M. M. Sanghvi, F. Zemrak, K. Fung, J. M. Paiva, V. Carapella, Y. J. Kim, H. Suzuki, B. Kainz, P. M. Matthews, S. E. Petersen, S. K. Piechnik, S. Neubauer, B. Glocker, D. Rueckert, Automated cardiovascular magnetic resonance image analysis with fully convolutional networks, J Cardiovasc Magn Reson 20 (1) (2018).

[24] B. Ruijsink, E. Puyol-Antón, I. Oksuz, M. Sinclair, W. Bai, J. A. Schnabel, R. Razavi, A. P. King, Fully Automated, Quality-Controlled Cardiac Analysis From CMR: Validation and Large-Scale Application to Characterize Cardiac Function, JACC Cardiovasc Imaging 13 (3) (2020) 684–695.

[25] K. Gilbert, W. Bai, C. Mauger, P. Medrano-Gracia, A. Suinesiaputra, A. M. Lee, M. M. Sanghvi, N. Aung, S. K. Piechnik, S. Neubauer, S. E. Petersen, D. Rueckert, A. A. Young, Independent left ventricular morphometric atlases show consistent relationships with cardiovascular risk factors: a UK Biobank study, Sci Rep 9 (1) (2019) 1–9.

[26] P. Medrano-Gracia, B. R. Cowan, B. Ambale-Venkatesh, D. A. Bluemke, J. Eng, J. P. Finn, C. G. Fonseca, J. A. C. Lima, A. Suinesiaputra, A. A. Young, Left ventricular shape variation in asymptomatic populations: The multi-ethnic study of atherosclerosis, J Cardiovasc Magn Reson 16 (2014) 1–10.

[27] K. Shameer, K. W. Johnson, B. S. Glicksberg, J. T. Dudley, P. P. Sengupta, Machine learning in cardiovascular medicine: Are we there yet?, Heart 104 (2018) 1156–1164.

[28] J. A. M. Sidey-Gibbons, C. J. Sidey-Gibbons, Machine learning in medicine: a practical introduction, BMC Med Res Methodol 19 (2019) 64.

[29] B. Ambale-Venkatesh, K. Yoneyama, R. K. Sharma, Y. Ohyama, C. O. Wu, G. L. Burke, S. Shea, A. S. Gomes, A. A. Young, D. A. Bluemke, J. A. C. Lima, Left ventricular shape predicts different types of cardiovascular events in the general population, Heart 103 (2017) 499–507.

[30] G. Farrar, A. Suinesiaputra, K. Gilbert, J. C. Perry, S. Hegde, A. Marsden, A. A. Young, J. H. Omens, A. D. McCulloch, Atlas-based ventricular shape analysis for understanding congenital heart disease, Prog Pediatr Cardiol 43 (2016) 61–69.

[31] C. Mauger, K. Gilbert, A. M. Lee, M. M. Sanghvi, N. Aung, K. Fung, V. Carapella, S. K. Piechnik, S. Neubauer, S. E. Petersen, A. Suinesiaputra, A. A. Young, Right ventricular shape and function: cardiovascular magnetic resonance reference morphology and biventricular risk factor morphometrics in UK biobank, J Cardiovasc Magn Reson 21 (2019) 1–13.

[32] B. Leonardi, A. M. Taylor, T. Mansi, I. Voigt, M. Sermesant, X. Pennec, N. Ayache, Y. Boudjemline, G. Pongiglione, Computational modelling of the right ventricle in repaired tetralogy of fallot: Can it provide insight into patient treatment?, Eur Heart J Cardiovasc Imaging 14 (2013) 381–386.

[33] T. Mansi, I. Voigt, B. Leonardi, X. Pennec, S. Durrleman, M. Sermesant, H. Delingette, A. M. Taylor, Y. Boudjemline, G. Pongiglione, N. Ayache, A statistical model for quantification and prediction of cardiac remodelling: Application to tetralogy of fallot, IEEE Trans Med Imaging 30 (2011) 1605–1616.

[34] K. Gilbert, N. Forsch, S. Hegde, C. Mauger, J. H. Omens, J. C. Perry, B. Pontré, A. Suinesiaputra, A. A. Young, A. D. McCulloch, Atlas-based computational analysis of heart shape and function in congenital heart disease, J Cardiovasc Transl Res 11 (2) (2018) 123–132.

[35] J. K. Shade, M. J. Cartoski, P. Nikolov, A. Prakosa, A. Doshi, E. Binka, L. Olivieri, P. M. Boyle, P. J. Spevak, N. A. Trayanova, Ventricular arrhythmia risk prediction in repaired tetralogy of fallot using personalized computational cardiac models, Heart Rhythm 17 (2020) 408–414.

[36] N. A. Trayanova, Your personal virtual heart, IEEE Spectr 51 (2014) 34–59.

[37] A. L. Marsden, J. A. Feinstein, Computational modeling and engineering in pediatric and congenital heart disease, Curr Opin Pediatr 27 (2015) 587–596.

[38] A. Updegrove, N. M. Wilson, J. Merkow, H. Lan, A. L. Marsden, S. C. Shadden, SimVascular: An open source pipeline for cardiovascular simulation, Ann Biomed Eng 45 (2017) 525–541.

[39] J. Corral-Acero, F. Margara, M. Marciniak, C. Rodero, F. Loncaric, Y. Feng, A. Gilbert, J. F. Fernandes, H. A. Bukhari, A. Wajdan, M. Villegas-Martinez, M. S. Santos, M. Shamohammdi, H. Luo, P. Westphal, P. Leeson, P. Diachille, V. Gurev, M. Mayr, L. Geris, P. Pathmanathan, T. Morrison, R. Cornelussen, F. Prinzen, T. Delhaas, A. Doltra, M. Sitges, E. Vigmond, E. Zacur, V. Grau, B. Rodriguez, E. W. Remme, S. Niederer, P. Mortier, K. Mcleod, M. Potse, E. Pueyo, A. Bueno-Orovio, P. Lamata, The "digital twin" to enable the vision of precision cardiology frontiers in cardiovascular medicine, Eur Heart J 0 (2020) 1–11.

[40] R. Altman, Artificial intelligence (AI) systems for interpreting complex medical datasets, Clin Pharmacol Ther 101 (2017) 585–586.

[41] J. H. Caufield, D. A. Liem, A. O. Garlid, Y. Zhou, K. Watson, A. A. T. Bui, W. Wang, P. Ping, A metadata extraction approach for clinical case reports to enable advanced understanding of biomedical concepts, J Vis Exp (2018).

[42] K. Benitez, B. Malin, Evaluating re-identification risks with respect to the HIPAA privacy rule, J Am Med Informatics Assoc 17 (2010) 169–177.

[43] L. Ohno-Machado, V. Bafna, A. A. Boxwala, B. E. Chapman, W. W. Chapman, K. Chaudhuri, M. E. Day, C. Farcas, N. D. Heintzman, X. Jiang, H. Kim, J. Kim, M. E. Matheny, F. S. Resnic, S. A. Vinterbo, W. Armstrong, N. Balac, J. Burns, J. Chen, R. Chisholm, R. Cope, S. Dasgupta, C. Dwork, R. El-Kareh, F. Fitzhenry, A. Gamst, A. Gentili, P. Good, A. Gupta, M. Inoue, R. Joyce, I. Krueger, G. Kuo, J. Larkin, K. Messer, L. Nookala, G. Norman, K. Norris, K. Patel, P. Paul, P. Pevzner, K. Patrick, S. Pond, J. Que, S. Rathbun, S. Robbins, A. Sarwate, C. Shimizu, H. Sofia, P. Tarczy-Hornoch, D. Thornton, F. Vaida, F. Valafar, G. Varghese, N. Wolter, C. Wong, M. Wong, A. Zambon, iDASH: Integrating data for analysis, anonymization, and sharing, J Am Med Informatics Assoc 19 (2012) 196–201.

[44] C. G. Fonseca, M. Backhaus, D. A. Bluemke, R. D. Britten, J. D. Chung, B. R. Cowan, I. D. Dinov, J. P. Finn, P. J. Hunter, A. H. Kadish, D. C. Lee, J. A. Lima, P. Medrano-Gracia, K. Shivkumar, A. Suinesiaputra, W. Tao, A. A. Young, The Cardiac Atlas Project-an imaging database for computational modeling and statistical atlases of the heart, Bioinformatics 27 (16) (2011) 2288–2295.

[45] C. Bentley, S. Cressman, K. van der Hoek, K. Arts, J. Dancey, S. Peacock, Conducting clinical trials—costs, impacts, and the value of clinical trials networks: A scoping review, Clin Trials 16 (2019) 183–193.

[46] N. Dłuzniewska, P. Podolec, M. Skubera, M. Smaś-Suska, J. Pajak, M. Urbańczyk-Zawadzka, W. Płazak, M. Olszowska, L. Tomkiewicz-Pajak, Long-term follow-up in adults after tetralogy of fallot repair, Cardiovasc Ultrasound 16 (2018).

[47] E. Garfield, The history and meaning of the journal impact factor, J Am Med Assoc 295 (2006) 90–93.

[48] D. A. Luke, C. C. Sarli, A. M. Suiter, B. J. Carothers, T. B. Combs, J. L. Allen, C. E. Beers, B. A. Evanoff, The translational science benefits model: A new framework for assessing the health and societal benefits of clinical and translational sciences, Clin Transl Sci 11 (2018) 77–84.

[49] M. Gurvitz, K. M. Burns, R. Brindis, C. S. Broberg, C. J. Daniels, S. M. Fuller, M. A. Honein, P. Khairy, K. S. Kuehl, M. J. Landzberg, W. T. Mahle, Emerging research directions in adult congenital heart disease: a report from an NHLBI/ACHA working group, JAMA Cardiol 67 (16) (2016) 1956–1964.

[50] M. E. Brickner, L. D. Hillis, R. A. Lange, Congenital heart disease in adults, New Engl J Med 342 (5) (2000) 334–342.

[51] J. A. Aboulhosn, G. Lluri, M. Z. Gurvitz, P. Khairy, F. P. Mongeon, J. Kay, A. M. Valente, M. G. Earing, A. R. Opotowsky, G. Lui, D. R. Gersony, Left and right ventricular diastolic function in adults with surgically repaired tetralogy of fallot: a multi-institutional study, Can J Cardiol 29 (7) (2013) 866–872.

[52] C. S. Broberg, J. Aboulhosn, F. P. Mongeon, J. Kay, A. M. Valente, P. Khairy, M. G. Earing, A. R. Opotowsky, G. Lui, D. R. Gersony, S. Cook, Prevalence of left ventricular

systolic dysfunction in adults with repaired tetralogy of fallot, Am J Cardiol 107 (8) (2011) 1215–1220.

[53] P. Khairy, J. Aboulhosn, M. Z. Gurvitz, A. R. Opotowsky, F. P. Mongeon, J. K. A. M. V. M. G. Earing, G. Lui, D. R. Gersony, S. C. S, Arrhythmia burden in adults with surgically repaired tetralogy of fallot: a multi-institutional study, Circulation 122 (9) (2010) 868–875.

[54] A. M. Valente, K. Gauvreau, G. E. Assenza, S. V. B.-N. SV, J. Schreier, M. A. Gatzoulis, M. Groenink, R. Inuzuka, P. J. Kilner, Z. Koyak, M. J. Landzberg, Contemporary predictors of death and sustained ventricular tachycardia in patients with repaired tetralogy of fallot enrolled in the INDICATOR cohort, Heart 100 (3) (2014) 247–253.

[55] J. Villafañe, J. A. Feinstein, K. J. Jenkins, R. N. Vincent, E. P. Walsh, A. M. Dubin, T. Geva, J. A. Towbin, M. S. Cohen, C. Fraser, J. Dearani, Hot topics in tetralogy of fallot, JAMA Cardiol 62 (23) (2013) 2155–2166.

[56] W. J. Krzanowski, Between-groups comparison of principal components, J Am Stat Assoc 74 (367) (1979) 703–707.

[57] A. Krishnamurthy, C. T. Villongco, J. Chuang, L. R. Frank, V. Nigam, E. Belezzuoli, P. Stark, D. E. Krummen, S. Narayan, J. H. Omens, A. D. McCulloch, Patient-specific models of cardiac biomechanics, J Comput Phys 244 (2013) 4–21.

[58] G. Nollert, T. Fischlein, S. Bouterwek, C. Böhmer, W. Klinner, B. Reichart, Long-term survival in patients with repair of tetralogy of fallot: 36-year follow-up of 490 survivors of the first year after surgical repair, J Am Coll Cardiol 30 (5) (1997) 1374–1383.

[59] N. M. Ammash, J. A. Dearani, H. M. Burkhart, H. M. Connolly, Pulmonary regurgitation after tetralogy of fallot repair: clinical features, sequelae, and timing of pulmonary valve replacement, Congenit Heart Dis 2 (6) (2007) 386–403.

[60] N. Tzemos, L. Harris, S. Carasso, L. Dos Subira, M. Greutmann, Y. Provost, A. N. Redington, H. Rakowski, S. C. Siu, C. K. Silversides, Adverse left ventricular mechanics in adults with repaired tetralogy of fallot, Am J Cardiol 103 (3) (2009) 420–425.

[61] A. Kempny, G.-P. Diller, S. Orwat, G. Kaleschke, G. Kerckhoff, A. C. Bunck, D. Maintz, H. Baumgartner, Right ventricular–left ventricular interaction in adults with tetralogy of fallot: a combined cardiac magnetic resonance and echocardiographic speckle tracking study, Int J Cardiol 154 (3) (2012) 259–264.

[62] T. Geva, B. Mulder, K. Gauvreau, S. V. Babu-Narayan, R. M. Wald, K. Hickey, A. J. Powell, M. A. Gatzoulis, A. M. Valente, Preoperative predictors of death and sustained ventricular tachycardia after pulmonary valve replacement in patients with repaired tetralogy of fallot enrolled in the indicator cohort, Circulation 138 (19) (2018) 2106–2115.

[63] S. Orwat, G.-P. Diller, A. Kempny, R. Radke, B. Peters, T. Kühne, D. Boethig, M. Gutberlet, K.-O. Dubowy, P. Beerbaum, et al., Myocardial deformation parameters predict outcome in patients with repaired tetralogy of fallot, Heart 102 (3) (2016) 209–215.

[64] G.-P. Diller, A. Kempny, E. Liodakis, R. Alonso-Gonzalez, R. Inuzuka, A. Uebing, S. Orwat, K. Dimopoulos, L. Swan, W. Li, et al., Left ventricular longitudinal function predicts life-threatening ventricular arrhythmia and death in adults with repaired tetralogy of fallot, Circulation 125 (20) (2012) 2440–2446.

[65] A. Ghai, C. Silversides, L. Harris, G. D. Webb, S. C. Siu, J. Therrien, Left ventricular dysfunction is a risk factor for sudden cardiac death in adults late after repair of tetralogy of fallot, Journal of the American College of Cardiology 40 (9) (2002) 1675–1680.

[66] A. L. Knauth, K. Gauvreau, A. J. Powell, M. J. Landzberg, E. P. Walsh, J. E. Lock, P. J. del Nido, T. Geva, Ventricular size and function assessed by cardiac mri predict major adverse clinical outcomes late after tetralogy of fallot repair, Heart 94 (2) (2008) 211–216.

[67] R. M. Wald, A. M. Valente, K. Gauvreau, S. V. Babu-Narayan, G. E. Assenza, J. Schreier, M. A. Gatzoulis, P. J. Kilner, Z. Koyak, B. Mulder, et al., Cardiac magnetic resonance markers of progressive rv dilation and dysfunction after tetralogy of fallot repair, Heart 101 (21) (2015) 1724–1730.

[68] L. Jing, G. J. Wehner, J. D. Suever, R. J. Charnigo, S. Alhadad, E. Stearns, D. Mojsejenko, C. M. Haggerty, K. Hickey, A. M. Valente, et al., Left and right ventricular dyssynchrony and strains from cardiovascular magnetic resonance feature tracking do not predict deterioration of ventricular function in patients with repaired tetralogy of fallot, J Cardiovasc Magn Reson 18 (1) (2016) 49.

[69] A. C. Andrade, M. Jerosch-Herold, P. Wegner, D. D. Gabbert, I. Voges, M. Pham, R. Shah, J. Hedderich, H.-H. Kramer, C. Rickers, Determinants of left ventricular dysfunction and remodeling in patients with corrected tetralogy of fallot, J Am Heart Assoc 8 (17) (2019).

[70] X. Zhang, B. R. Cowan, D. A. Bluemke, J. P. Finn, C. G. Fonseca, A. H. Kadish, D. C. Lee, J. A. Lima, A. Suinesiaputra, A. A. Young, et al., Atlas-based quantification of cardiac remodeling due to myocardial infarction, PloS One 9 (10) (2014).

[71] S. Holm, A simple sequentially rejective multiple test procedure, Scand J Stat (1979) 65–70.

[72] P. C. Mahalanobis, On the generalized distance in statistics, National Institute of Science of India, 1936.

[73] T. Kono, H. N. Sabbah, H. Rosman, M. Alam, S. Jafri, S. Goldstein, Left ventricular shape is the primary determinant of functional mitral regurgitation in heart failure, J Am Coll Cardiol 20 (7) (1992) 1594–1598.

[74] A. Ganau, R. B. Devereux, M. J. Roman, G. De Simone, T. G. Pickering, P. S. Saba, P. Vargiu, I. Simongini, J. H. Laragh, Patterns of left ventricular hypertrophy and geometric remodeling in essential hypertension, J Am Coll of Cardiol 19 (7) (1992) 1550–1558.

[75] F. Li, Y. G. Chen, G. H. Yao, L. Li, Z. M. Ge, M. Zhang, Y. Zhang, Usefulness of left ventricular conic index measured by real-time three-dimensional echocardiography to predict left ventricular remodeling after acute myocardial infarction, Am J Cardiol 102 (11) (2008) 1433–1437.

[76] S. Babu-Narayan, P. Kilner, W. Li, J. Moon, O. Goktekin, P. Davlouros, et al., Ventricular fibrosis suggested by cardiovascular magnetic resonance in adults with repaired congenital heart disease: value of mr imaging in comparison to echocardiography, Pediatr Radiol 37 (2007) 426–436.

[77] R. M. Wald, I. Haber, R. Wald, A. M. Valente, A. J. Powell, T. Geva, Effects of regional dysfunction and late gadolinium enhancement on global right ventricular function and exercise capacity in patients with repaired tetralogy of fallot, Circulation 119 (10) (2009) 1370–1377.

[78] C.-A. Chen, S. M. Dusenbery, A. M. Valente, A. J. Powell, T. Geva, Myocardial ecv fraction assessed by cmr is associated with type of hemodynamic load and arrhythmia in repaired tetralogy of fallot, JACC Cardiovasc Imaging 9 (1) (2016) 1–10.

[79] C. S. Broberg, J. Huang, I. Hogberg, J. McLarry, P. Woods, L. J. Burchill, G. A. Pantely, D. J. Sahn, M. Jerosch-Herold, Diffuse lv myocardial fibrosis and its clinical associations in adults with repaired tetralogy of fallot, JACC Cardiovasc Imaging 9 (1) (2016) 86–87.

[80] S.-n. Li, W. Yu, C. T.-m. Lai, S. J. Wong, Y.-f. Cheung, Left ventricular mechanics in repaired tetralogy of fallot with and without pulmonary valve replacement: analysis by three-dimensional speckle tracking echocardiography, PLoS One 8 (11) (2013).

[81] Q. A. Hagdorn, J. D. Vos, N. E. Beurskens, T. M. Gorter, S. L. Meyer, J. P. van Melle, R. M. Berger, T. P. Willems, Cmr feature tracking left ventricular strain-rate predicts ventricular tachyarrhythmia, but not deterioration of ventricular function in patients with repaired tetralogy of fallot, Int J Cardiol 295 (2019) 1–6.

[82] M. D. Samad, G. J. Wehner, M. R. Arbabshirani, L. Jing, A. J. Powell, T. Geva, C. M. Haggerty, B. K. Fornwalt, Predicting deterioration of ventricular function in patients with repaired tetralogy of fallot using machine learning, Eur Heart J Card Img 19 (7) (2018) 730–738.

[83] K. Gilbert, B. Pontre, C. Occleshaw, B. Cowan, A. Suinesiaputra, A. Young, 4d modelling for rapid assessment of biventricular function in congenital heart disease, Int J Cardiovas Imag 34 (3) (2018) 407–417.

[84] H. Latus, P. Hachmann, K. Gummel, M. Khalil, C. Yerebakan, J. Bauer, D. Schranz, C. Apitz, Impact of residual right ventricular outflow tract obstruction on biventricular strain and synchrony in patients after repair of tetralogy of fallot: a cardiac magnetic resonance feature tracking study, European Journal of Cardio-Thoracic Surgery 48 (1) (2015) 83–90.

[85] S. Klotz, I. Hay, M. L. Dickstein, G.-H. Yi, J. Wang, M. S. Maurer, D. A. Kass, D. Burkhoff, Single-beat estimation of end-diastolic pressure-volume relationship: a novel method with potential for noninvasive application, American Journal of Physiology-Heart and Circulatory Physiology 291 (1) (2006) H403–H412.

[86] F. P. Fernandes, C. Manlhiot, S. L. Roche, L. Grosse-Wortmann, C. Slorach, B. W. Mc-Crindle, L. Mertens, P. F. Kantor, M. K. Friedberg, Impaired left ventricular myocardial mechanics and their relation to pulmonary regurgitation, right ventricular enlargement and exercise capacity in asymptomatic children after repair of tetralogy of Fallot, J Am Soc Echocardiogr 25 (5) (2012) 494–503.

[87] A. Dragulescu, M. K. Friedberg, L. Grosse-Wortmann, A. Redington, L. Mertens, Effect of chronic right ventricular volume overload on ventricular interaction in patients after tetralogy of fallot repair, J Am Soc Echocardiogr 27 (8) (2014) 896–902.

[88] A. Nakamura, H. Horigome, Y. Seo, T. Ishizu, R. Sumazaki, Right ventricular remodeling due to pulmonary regurgitation is associated with reduced left ventricular free wall strain in surgically repaired tetralogy of Fallot, Circulation 78 (8) (2014) 1960–1966.

[89] A. E. van der Hulst, V. Delgado, E. R. Holman, L. J. Kroft, A. de Roos, M. G. Hazekamp, N. A. Blom, J. J. Bax, A. A. Roest, Relation of left ventricular twist and global strain with right ventricular dysfunction in patients after operative "correction" of tetralogy of fallot, Am J Cardiol 106 (5) (2010) 723–729.

[90] E. W. Cheung, X.-c. Liang, W. W. Lam, Y.-f. Cheung, Impact of right ventricular dilation on left ventricular myocardial deformation in patients after surgical repair of tetralogy of fallot, Am J Cardiol 104 (9) (2009) 1264–1270.

[91] F. H. Sheehan, S. Ge, G. W. Vick III, K. Urnes, W. S. Kerwin, E. L. Bolson, T. Chung, J. P. Kovalchin, D. J. Sahn, M. Jerosch-Herold, et al., Three-dimensional shape analysis of right ventricular remodeling in repaired tetralogy of fallot, Am J Cardiol 101 (1) (2008) 107–113.

[92] H. Zhang, A. Wahle, R. K. Johnson, T. D. Scholz, M. Sonka, 4-d cardiac mr image analysis: left and right ventricular morphology and function, IEEE Transactions on Medical Imaging 29 (2) (2009) 350–364.

[93] P. Ylitalo, E. Jokinen, K. Lauerma, M. Holmström, O. M. Pitkänen-Argillander, Additional mechanism for left ventricular dysfunction: chronic pulmonary regurgitation decreases left ventricular preload in patients with tetralogy of fallot, Cardiology in the Young 28 (2) (2018) 208–213.

[94] S. Babu-Narayan, P. Kilner, W. Li, J. Moon, O. Goktekin, P. Davlouros, et al., Ventricular fibrosis suggested by cardiovascular magnetic resonance in adults with repaired tetralogy of fallot and its relationship to adverse markers of clinical outcome, Circulation 113 (3) (2006) 405–413.

[95] G. A. Holzapfel, R. W. Ogden, Constitutive modelling of passive myocardium: a structurally based framework for material characterization, Philosophical Transactions of the Royal Society A: Mathematical, Physical and Engineering Sciences 367 (1902) (2009) 3445–3475.